MIXING ENERGY ANALYSIS OF BINGHAM PLASTIC FLUIDS FOR

SEVERE LOST CIRCULATION PREVENTION USING SIMILITUDE

A Thesis

by

ROBERT DERRYL MASSINGILL, JR.

Submitted to the Office of Graduate Studies of
Texas A&M University
in partial fulfillment of the requirements for the degree of

MASTER OF SCIENCE

May 2005

Major Subject: Petroleum Engineering

MIXING ENERGY ANALYSIS OF BINGHAM PLASTIC FLUIDS FOR

SEVERE LOST CIRCULATION PREVENTION USING SIMILITUDE

A Thesis

by

ROBERT DERRYL MASSINGILL, JR.

Submitted to Texas A&M University
in partial fulfillment of the requirements
for the degree of

MASTER OF SCIENCE

Approved as to style and content by:

| Jerome J. Schubert | Hans C. Juvkam-Wold |
| (Chair of Committee) | (Member) |

| William C. Schneider | Stephen A. Holditch |
| (Member) | (Head of Department) |

May 2005

Major Subject: Petroleum Engineering

ABSTRACT

Mixing Energy Analysis of Bingham Plastic Fluids for Severe Lost Circulation

Prevention Using Similitude.

(May 2005)

Robert Derryl Massingill, Jr., B.S., Texas A&M University

Chair of Advisory Committee: Dr. Jerome J. Schubert

As the demand for oil and gas resources increases, the need to venture into more hostile environments becomes a dynamic focus in the petroleum industry. One problem associated with certain high risk formations is lost circulation. As a result, engineers have concentrated research efforts on developing novel Lost Circulation Materials (LCM's) that will effectively treat thief zones. The most pioneering LCM's require mixing energy to activate a reaction involving two or more chemicals. However, minimal research has been conducted to accurately predict downhole mixing capabilities. Therefore, this research focuses on developing a correlation between laboratory experiments and scaled model experiments for accurate prediction of downhole mixing energies in terms of flow rate for adequate mixing of lost circulation prevention fluids.

DEDICATION

This work is dedicated to several people who have influenced my life. First, I would like to thank Jesus for always shining in my heart to show me the proper paths to take.

I would also like to thank my loving grandparents, Robert and Tommie Massingill (Punkin and Memaw), for their understanding and support throughout my life. They have made all of my dreams come true and have helped me realize that a world full of opportunity truly does exist.

Antoinette Hernandez, my girlfriend, has supported me throughout all of my college adventures and has given me hope when times were at their worst.

My father, Robert D. Massingill, Sr., has been my best friend and has offered advice when major decisions burdened me.

My mother, Margaret Moore, gave me the courage to pursue a life of good fortune.

Finally, I would like to thank my brothers for giving me an opportunity to show them that dreams can come true.

ACKNOWLEDGEMENTS

TABLE OF CONTENTS

LIST OF FIGURES

Page

LIST OF TABLES

CHAPTER I

INTRODUCTION

Increasing consumption of oil and gas from industrializing nations along with escalated prices has led to intensifying efforts to recover newly discovered and once abandoned hydrocarbons. It is known throughout the industry that conventional or easy to obtain reservoirs are rapidly disappearing and more difficult unconventional reservoirs are stealing the spotlight. Although many of the hydrocarbons have been recovered from conventional reservoirs, drilling programs are continually being executed into depleted formations. One of the most cumbersome problems associated with drilling both unconventional reservoirs and depleted zones is lost circulation. It has been determined that lost circulation occurs primarily in fractured formations, both natural and induced, or in areas of exceptionally high permeability, characteristic of loosely compacted formations.[1-4] In addition, the severity of the loss is determined by the characteristics of the loss zone. The primary problem associated with depleted reservoirs is the decline in rock stress due to the reduction of pore pressure. According to Adachi *et al.*[5], "the issue of drilling depleted zones is increasing in importance as more wells are drilled in mature fields".

This thesis follows the style of the *SPE Drilling and Completion*.

Even with the exponential growth in drilling technology, lost circulation does occur. In trying to understand the concept of lost returns, the industry has classified losses in terms of severity as: "1. seepage loss, when the severity of the loss is 1-10 bbl/hr; 2. partial loss, when the severity of the loss is 10-500 bbl/hr; [or] 3. complete loss, when the severity of the loss is 500 bbl/hr and over".[3] According to Messenger[6], the only acceptable quantities of fluid loss are less than 1 bbl/hr; although, many times treatment decisions are based on economic reasons. Treatment selections, on the other hand, are based on the mechanism of loss which may be matrix seepage, filtrate, vugular, or from fracture propagation.[7] This study is primarily concerned with losses occurring from fractured propagation.

Lost circulation occurs into fractures when the hydraulic pressure in the wellbore is slightly higher than the rocks stress holding the borehole closed. The excess pressure forces the wellbore to open in the direction perpendicular to the minimum in-situ stress field. Drilling fluid continues to flow into, and propagate the fracture as long as the wellbore pressure exceeds the rock stress that is attempting to force the two faces of the fracture to close. This stress is the minimum in-situ far field stress. Lost returns are stopped by reducing the fluid density so that the pressure in the wellbore is below the Fracture Closure Stress (FCS), or by building the FCS to exceed the wellbore pressure. The function of a lost returns treatment for fracture propagation type losses is to build FCS.[7]

By definition, "lost circulation is the partial or complete loss of drilling fluid or cement slurries into formations during drilling, circulation, running casing, or cementing

operations."[8,9] Some of the more hazardous problems that are indirectly associated with lost circulation are surface and underground blowouts, differential drill string sticking, and formation damage. It was reported that lost circulation occurs during drilling on approximately 20 to 25% of the wells drilled worldwide.[10] As can be imagined, hundreds of millions, if not billions, of dollars each year are spent on the ever growing problem.

As drilling continues to increase in high risk formations, efforts have been focused on developing new Lost Circulation Materials (LCM's) that are more effective and that minimize the operation costs by achieving sufficient FCS to allow drilling to continue.[7,8] A variety of products have been proposed with a range of complexities and applications. Some novel formulations require adequate downhole mixing while others are simply pumped into the accepting formations. It has been reported that, "LCM's are often used to form a filter cake, which impedes fluid flow into thief zones".[11] This is correct for matrix seepage losses; however, LCM's used to stop the fracture propagation process must have additional attributes. Surprisingly, minimal research has been conducted to accurately predict actual downhole mixing capabilities of viscous fluids so that the state of the materials as they enter the fracture can be predicted. As a result, this study focuses on developing correlations between laboratory experiments and field applications concerning two-stream jet mixing.

CHAPTER II

LITERATURE REVIEW

2.1 Present Status of Lost Circulation Materials

Lost circulation has been a major concern of the petroleum industry, and continues to affect drilling operations around the world. In the industry's infancy, lost circulation was not well understood and often times led to more serious well control problems. Engineers quickly began studying the phenomenon and developing preventive products. Early LCM's could be classified into four groups: fibrous LCM's, flake LCM's, granular LCM's, and blended LCM's.[3,4,9] These products consisted largely of solids such as shells, sea weed, tree bark, raw cotton, etc. that could be pumped into the thief zones.[3,4] Some of the afore mentioned products are still used today to combat seepage or filtrate losses; however, some lost circulation events require more innovative materials to regain full returns. Since the time of desperate measures to control the fluid losses, more technologically advanced chemical lost circulation treatments have emerged that focus on rapid application and effectively widening the mud weight window, therefore, minimizing drilling costs.

Among the most popular LCM's used while treating minor lost circulations are blended combinations of particulates. It has been reported that clay and other solids used for lost circulation purposes are effective if the pore size or fracture width to be sealed is less than about three times the diameter of the largest particles present.[12] Numerous studies have been conducted that were directed toward developing the most

efficient combinations of solids suitable for bridging and sealing thief zones.[3,4,9,13-17] It has been determined that blended LCM's minimize filter cake permeability to stop matrix seepage losses and provide sufficient post-treatment structural integrity by offering particles of varying sizes and compressive strengths. The use of particulates remains one of the most researched and widely accepted practices for both matrix seepage and fracture propagation losses.

In addition to particulate LCM's, specialized cementing practices are also often implemented to control lost circulation.[8,11,18-22] However, cement applications do have limitations. One such limitation is that cement plugs are permanent and irreversible in many cases. Therefore, the technique is usually applied to non-producing zones, in which mud loss is extremely severe, as a quick and permanent remedy.[8] However, if cement must be used in productive zones, then care must be taken to ensure adequate solubility by later acid treatments, or the completion scheme must include plans to perforate through the plugged rock face.[23,24] As a result of the many problems associated with cement uses in lost circulation applications, it is usually not a preferred approach for many lost returns events.

Despite the variety of the products that are available, there continues to be a need for materials that are more effective and predictable in their ability to cure fracture propagation lost circulation. Therefore, impressive efforts have been geared toward developing chemical LCM's that provide an easy and effective solution that does not cause permanent damage to the well, and that works uniformly in a wide range of applications.[1,11,13,25] One of the earliest LCM's utilized a bentonite-diesel combination

that formed a pliable product of stiff consistency when mixed with mud or water.[26-28] Another such chemical method for formation plugging involves three products that vigorously react to form a polymer acceptable for plugging pore space or induced fracture volume.[11] In 1984, Halliburton developed a similar product, referred to as FC.[1]

Perhaps the most innovative products are those that require a specified amount of downhole mixing or involve crosslinkers.[13,25,29-32] In 1985, Exxon Production Research Co. published an article proposing a shear-thickening fluid for stopping unwanted flows.[25] The properties of the fluid allow it to remain in a low viscosity state until it has been subjected to high levels of shearing. In 2003, Halliburton developed a similar product, referred to as CCF, that utilized the downhole mixing capabilities of a two-stream system.[13] Furthermore, CCF seems to be activated by shearing as well. The most recent advancement in LCM's employs the use of cements coupled with a crosslinker.[29] The crosslinking agent in the product allows both productive and non-productive zones to be treated with minimal well damage. According to the Mata and Veiga, the crosslinked cement can exhibit up to 98% solubility.[29]

Although chemical LCM's appear to be the ultimate solution to lost circulation, problems do exist in downhole situations. According to Dupriest,[33] the LCM must have a high viscosity when pumped into the fracture to achieve the appropriate FCS. However, crosslinkers are often placed in the fracture at a low viscosity; consequently, the wellbore never builds sufficient integrity. Downhole mixing materials, on the other hand, achieve immediate high viscosity for proper fracture width propagation so that greater increases in FCS can be achieved.

Since most recent advancements in LCM technology to combat fracture propagation lost circulation seem to focus on downhole mixing of reactive products, it seems that research efforts aimed at understanding the actual downhole mixing capabilities are appropriate. Consequently, developing a model to simulate actual downhole mixing conditions will be the main objective of this work.

CHAPTER III

OBJECTIVES AND PROCEDURES

3.1 Research Objectives

The objectives of this research are as follows:

1. To design and implement a test matrix using mechanical agitation in a laboratory that will predict the flow rate required through a nozzle for adequate in-situ mixing of a two-stream chemical lost circulation treatment.

2. To design a scaled model of a drilling operation using similitude that will simulate downhole mixing capabilities using different flow rates of the two-stream system.

3. To develop a correlation between the laboratory experiments predicted flow rates and the scaled model experimental flow rates that can be used in field service operations.

3.2 Research Procedures

To accomplish the goals of this research project, the following procedures will be applied:

1. Conduct laboratory experiments using a foam cement blender to observe the yield point behavior of a Product based on Latex Inversion Process (PLIP) product.

2. Develop a similitude scaling spreadsheet to be used in designing a wellbore model apparatus.

3. Conduct tests in the wellbore model using PLIP and measure the yield point of the resultant product.

4. Compare the data obtained from steps 1 and 3, and obtain recommended flow rates for field application.

CHAPTER IV

EXPERIMENTAL DEVELOPMENT

4.1 Purpose

Current drilling practices require processing aids such as lost circulation materials to prevent fluid loss thus facilitating drilling as long as possible before setting casing. By setting unnecessary casing strings, excessive costs are incurred that could be avoided by widening the mud weight window.

Halliburton Energy Services has developed proprietary products such as PLIP that, when adequately mixed downhole, results in a unique material that has properties of plastic putty type sealants thus effectively preventing lost circulation caused by fracture propagation and allowing drilling to continue, consequently, minimizing non-productive time, casing costs, and cementing costs.

Lab results have shown that the type and amount of mixing affects the rheology of the reacted product. Currently, there are no specific engineering practices or lab models that simulate downhole mixing processes such that chemical formulation of PLIP and placement conditions can be optimized for mixing enlargement of the mud weight window.

The mixing energy involved in successfully placing PLIP lost circulation treatments is extremely important. The goal of this project was to perform an in-depth study of the actual downhole mixing energy associated with PLIP jet flow and to find the

minimum flow rate that creates a quality product. This analysis brings advanced scientific support to PLIP treatments.

4.2 Scope and Procedure

The purpose of PLIP, a unique product in Halliburton's DrillAhead® service, is to prevent severe lost circulation caused by fracture propagation via a two-stream downhole mixing process. The main benefit is the avoidance of setting casing and cementing the well. Severe lost circulation, defined for this study, is losing approximately 50 bbl/hr of drilling fluid to the formation. PLIP is a technology that, when given adequate downhole mixing, quickly develops into a stiff Bingham plastic type material with Yield Points (YP's) on the order of 2,000 lb/100ft^2 and up, thus providing a significant increase in an operators mud weight window when properly placed in an accepting fracture.

Since adequate downhole mixing is crucial to creating a quality product, then an analysis including a mathematical model, a laboratory method, and a pilot scale was developed. The objectives to complete the DrillAhead® mixing energy analysis project are described in **Fig. 1** and **Fig. 2**. Notice that the graphical analysis of the project objectives, shown in Fig. 2, demonstrates that the difficulty of the project is relating mixing by mechanical agitation to non-mechanical jet mixing

1. To design and implement a test matrix that uses mechanical agitation in a laboratory that will predict the flow rate required through a nozzle for adequate in-situ mixing of a two-stream chemical severe lost circulation treatment.

2. To design a scaled model of a drilling operation using similitude that will simulate downhole mixing capabilities using different flow rates of the two-stream system.

3. To develop a correlation between the laboratory experiments predicted flow rates and the scaled model experimental flow rates that can be used in field service operations.

Fig. 1 — Project objectives.
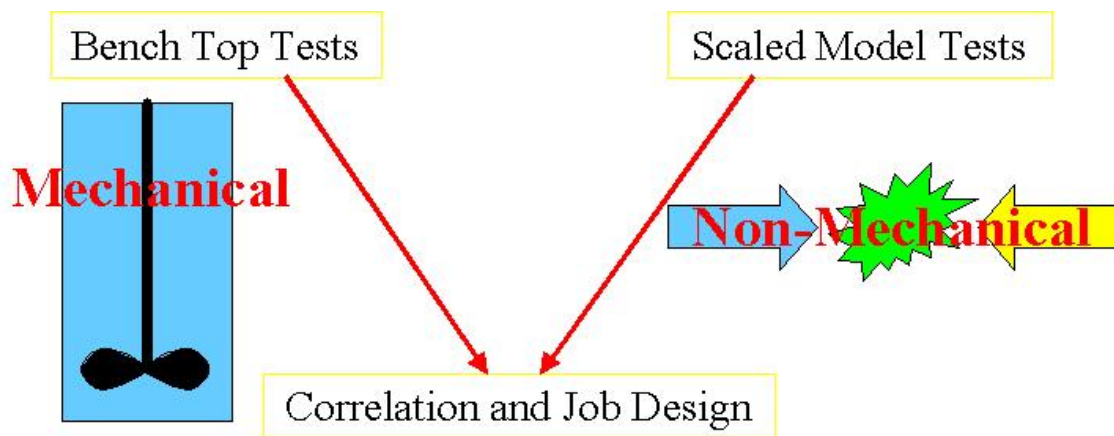
Fig. 2 — Graphical explanation of objectives.

4.3 Bench-Top Blender Tests

According to the first objective, mechanical agitation by way of a blender is used to begin to understand the amount of applied mixing energy required to obtain fully reacted acceptable product. The following discussion explains the apparatus, procedure, and data analysis pertaining to the bench-top blender tests.

4.3.1 Apparatus

The testing equipment used for the bench-top experiments consisted of a Manual Yield Point Device (MYPD) and a foam cement blender. The MYPD finds the YP for semi-solid materials with consistencies like that of peanut butter. A normal viscometer could not be used because the PLIP product has a similarly stout consistency. A description of and the procedure for the MYPD operation will be discussed later in greater detail.

The mixing apparatus includes a blender equipped with a time control and rheostat. The rheostat allows the blender to maintain a constant speed, and the time control ensures that the desired mixing times are achieved.
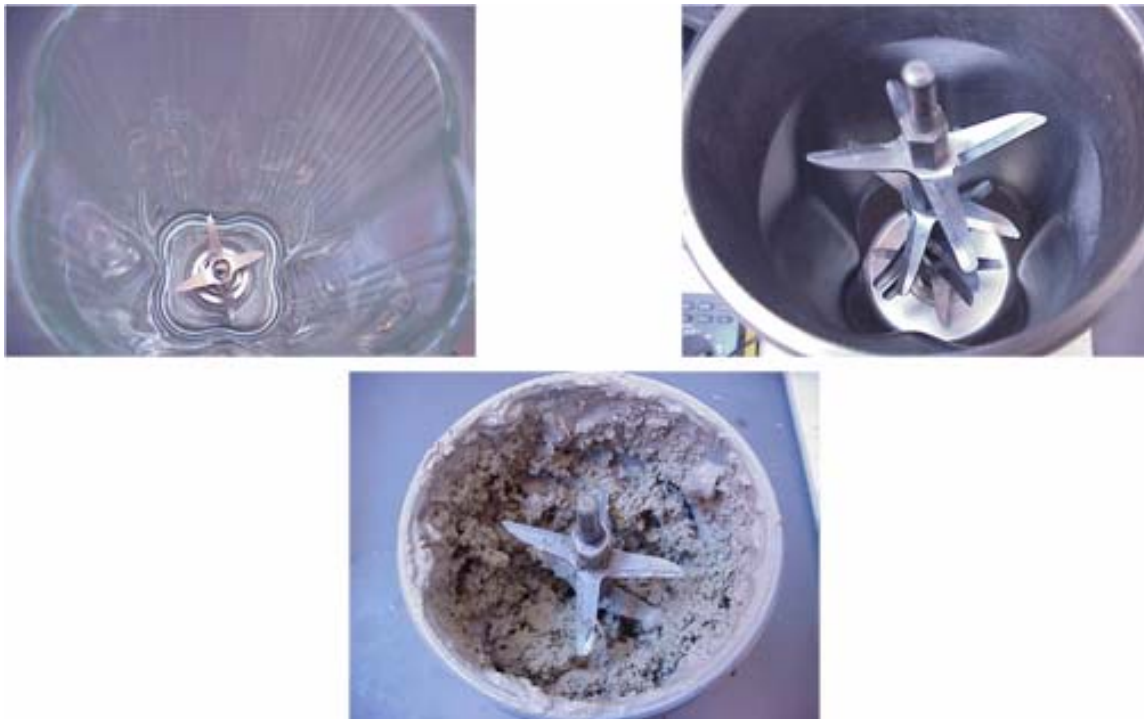
Fig. 3 — Blender comparison.

Every effort is made to improve the efficiency of testing procedures. While running some preliminary test with the Waring blender (top left of **Fig. 3**), it was observed that fully reacted sample collected around the blender blade while non-reacted sample lay on top. By using the foam cement blender with multiple blades (top right of Fig. 3), it was noticed that the entire sample reacted (bottom of Fig. 3).

4.3.2 Procedure

Note: Table 1 specifies the test matrix pertaining to this procedure.

1. Obtain equal amounts of PLIP and Oil Based Mud (OBM). 350 cc of each fluid were used for this analysis.

2. Set the blender to desired mixing times and RPM. **Note:** The RPMs listed in Table 1 are actual. The desired RPMs were 2,000; 4,000; 6,000; 8,000; and 10,000 rev/min.

3. Pour the OBM in the blender first, and then the PLIP. **Note:** It is important that this step be followed in order to best simulate actual conditions.

4. Immediately begin the mixing process by pressing the blender control start button.

5. Read the best represented RPM for the test.

6. Immediately empty the sample into a 32 oz bucket and pack for yield point testing.

Packing the sample is perhaps the most important aspect of testing the YP of the reacted product. All samples obtained in this experiment were packed according to the following guidelines presented in **Fig. 4**.

---

1. Place approximately 175 cc of the reacted product in a 32 oz bucket.
2. Flatten the reacted sample with your hand until there are no voids present.
3. Continue the process until the entire sample has been packed in the bucket.

Note: Since the PLIP is highly sensitive to shear, a conscious effort must be made to limit the amount a shear exposed to the sample during the packing process.

Fig. 4 — Packing procedure.

7. Measure the YP of the sample at 30 min curing time. **Note:** 30 min is the time span specified for a complete PLIP reaction.

The YP of each of the samples was obtained using the MYPD according to the following procedure outlined in **Fig. 5**.

---

1. After the sample is packed, insert the flag into the center of the sample approximately 1 ½ in.
2. Be sure that the dial on the MYPD crank is set to zero.
3. Place the sample on the jack and raise while simultaneously guiding the flag into the dial port.
4. Turn the MYPD weight gauge on and reset to zero ounces.
5. Rotate the dial crank approximately 1 rev/sec until the dial rotates about 90 deg.
6. Read the value from the weight gauge.

Fig. 5 — Yield point measurement procedure.

Table 1 — Fluid System A – Blender Test Matrix

Description	Value	Units
Volume	700	[cc]
Mass	1.092	[kg]
P-exponent	1	-
K_1	0.11	-
alpha	0.000105	
beta	1	-
Ypoo	3.3	[Ratio]

Hand Stir	
Yield Point	Units
0.10	[Ratio]
0	[RPM]

Test ID	Mixing Time	RPM	Shear Rate	ISH	Yield Point				
-	[sec]	-	[1/sec]	-	Measurements [Ounces]			Average	Predicted
					1	2	3	[Ratio]	[Ratio]
1	2	9610	1057.10	2114.20	6.50	7.10	6.10	0.69	-
2	5	9820	1080.20	5401.00	8.30	8.30	8.50	0.88	-
3	10	9500	1045.00	10450.00	13.50	14.10	13.60	1.45	-
4	15	9820	1080.20	16203.00	24.90	25.30	24.60	2.63	-
5	30	10000	1100.00	33000.00	29.90	30.00	31.50	3.21	-
6	2	7206	792.66	1585.32	6.00	6.10	6.20	0.64	0.60
7	5	7800	858.00	4290.00	11.10	10.80	11.00	1.16	1.27
8	10	8010	881.10	8811.00	17.90	16.50	17.10	1.81	2.06
9	15	7890	867.90	13018.50	20.60	21.30	21.60	2.23	2.52
10	30	7850	863.50	25905.00	24.60	25.10	24.80	2.62	3.13
11	2	5230	575.30	1150.60	4.90	4.10	4.50	0.47	0.47
12	5	5910	650.10	3250.50	7.10	7.80	7.40	0.78	1.04
13	10	5990	658.90	6589.00	14.30	14.70	14.50	1.53	1.72
14	15	5870	645.70	9685.50	14.40	15.80	15.10	1.59	2.17
15	30	5960	655.60	19668.00	21.40	21.20	20.60	2.22	2.93
16	2	3800	418.00	836.00	4.10	4.30	4.00	0.44	0.37
17	5	3860	424.60	2123.00	7.20	7.80	7.00	0.77	0.75
18	10	3990	438.90	4389.00	14.60	14.30	14.30	1.52	1.30
19	15	3920	431.20	6468.00	13.60	14.50	15.80	1.54	1.70
20	30	3890	427.90	12837.00	23.00	22.60	24.50	2.47	2.50
21	2	1810	199.10	398.20	2.10	2.00	1.90	0.21	0.23
22	5	1900	209.00	1045.00	3.30	3.00	3.20	0.33	0.44
23	10	2000	220.00	2200.00	6.90	6.50	6.50	0.70	0.77
24	15	1920	211.20	3168.00	10.60	9.20	9.50	1.03	1.02
25	30	1810	199.10	5973.00	22.20	24.00	23.70	2.46	1.61

4.3.3 Data Analysis

Note: Only data from the fluid system A experiments is presented in the discussion of this thesis. Experiments using other drilling fluids are placed in the appendices.

An important discovery in this project is that accumulated shear history is key to achieving a high YP. This theory can best be described by the following explanation.

Imagine a mixing barrel with a mixing crank filled with equal amounts of three different colored balls. If the crank is rotated one full revolution and the average ball moves two times its size, then the accumulated shear on that ball is 2. Note that the balls are still separated. If the crank is rotated one-thousand revolutions, then the accumulated shear on a ball is 2,000. Here, the balls are adequately mixed.

Accumulated shear history, termed as Integral Shear History (ISH), can be calculated from Eq. 1.

$$\text{ISH} = \int_{t_0}^{t} \dot{\gamma}^P \, dt = \dot{\gamma}^P \int_{t_o}^{t} dt = \dot{\gamma}^P \left[t - t_0 \right] = \dot{\gamma}^P t_{\text{mix}} \quad \text{.. (1)}$$

In Eq. 1, p represents the materials sensitivity to shear, and $\dot{\gamma}$ is the shear rate of the blender. According to Meier and Morgan[34], the shear rate of a blender, shown in Eq. 2, can be determined as a function of RPM, volume, geometry, and rheology.

$$\dot{\gamma} = K_1 \left(V_{\text{RPM}} \right) \quad \text{... (2)}$$

Using Meier and Morgan's study[34], it was determined that K_1 for the foam blender is approximately 0.11 as can be seen from the slope of the line in **Fig. 6**.
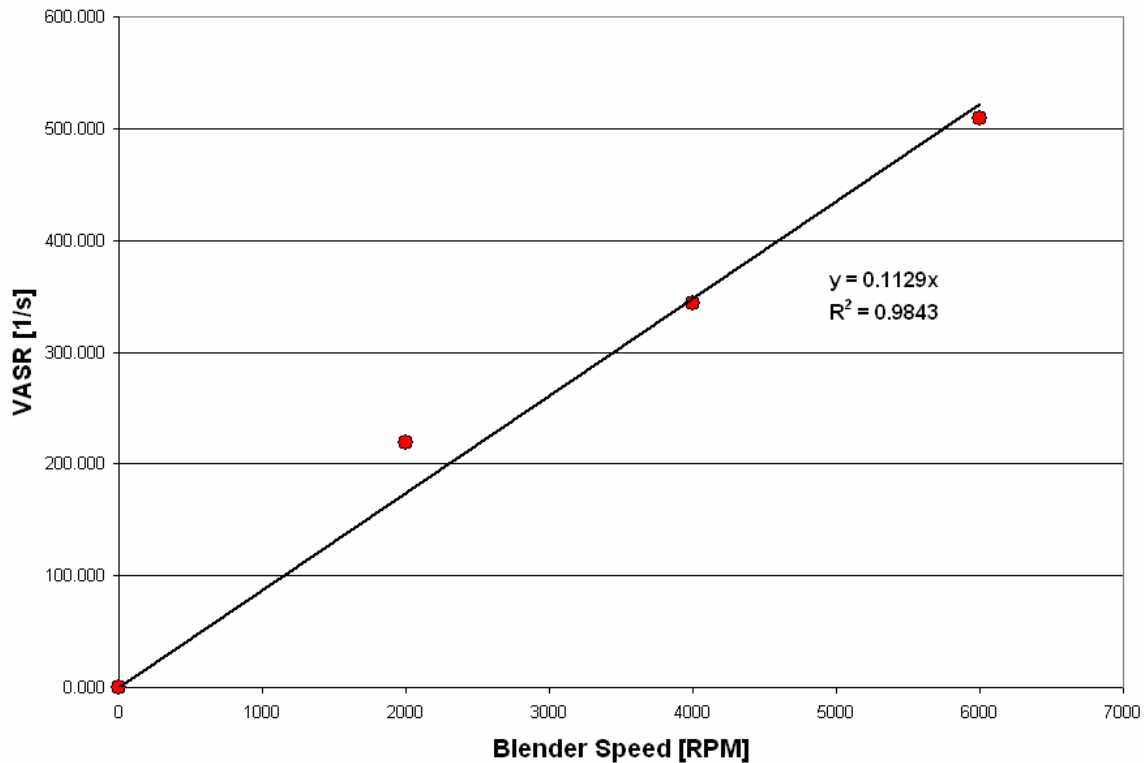
Fig. 6 — Shear rate constant correlation.

A classical first order model, shown in Eq. 3, is often used in predicting simple reactions. In the equation, Y_0 is an initial value, and Y_∞ is a final value of some measurable parameter of a material. Furthermore, k is referred to as the reaction constant that is specific to certain chemical reactions, and can be expressed in a wide range of values.

$$Y(X) = Y_0 + (Y_{max} - Y_0)(1 - e^{-kX})$$ .... (3)

The generalized rheological equation, shown in Eq. 4, was used to relate the ISH to YP. Notice that Eq. 4 introduces an additional parameter β. By modifying the classical first order model, more flexibility in representing complex reactions is

achieved. Therefore, data that does not necessarily respond as a first order reaction can be better characterized. **Table 2** offers a description of the parameters shown in Eq. 4.

$$YP(\text{ISH}) = YP_0 + (YP_\infty - YP_0)(1 - e^{-\alpha(\text{ISH})})^\beta \quad \text{... (4)}$$

Table 2 — Parameters for Generalized Rheological Model

Variable	Description	Units
YP_0	Initial Yield Point	[lb/100ft^2]
YP_∞	Final Yield Point	[lb/100ft^2]
α	Psuedo Rate Constant	-
β	Material Reaction Parameter	-

α determines the reaction rate of the mixture, and β represents the lag time until the reaction initiates. **Fig. 7** and **Fig. 8** show the effects of changing α and β individually while simultaneously holding the other constant. It can be determined from the figures that a variety of non-first order reactions can be accurately predicted.
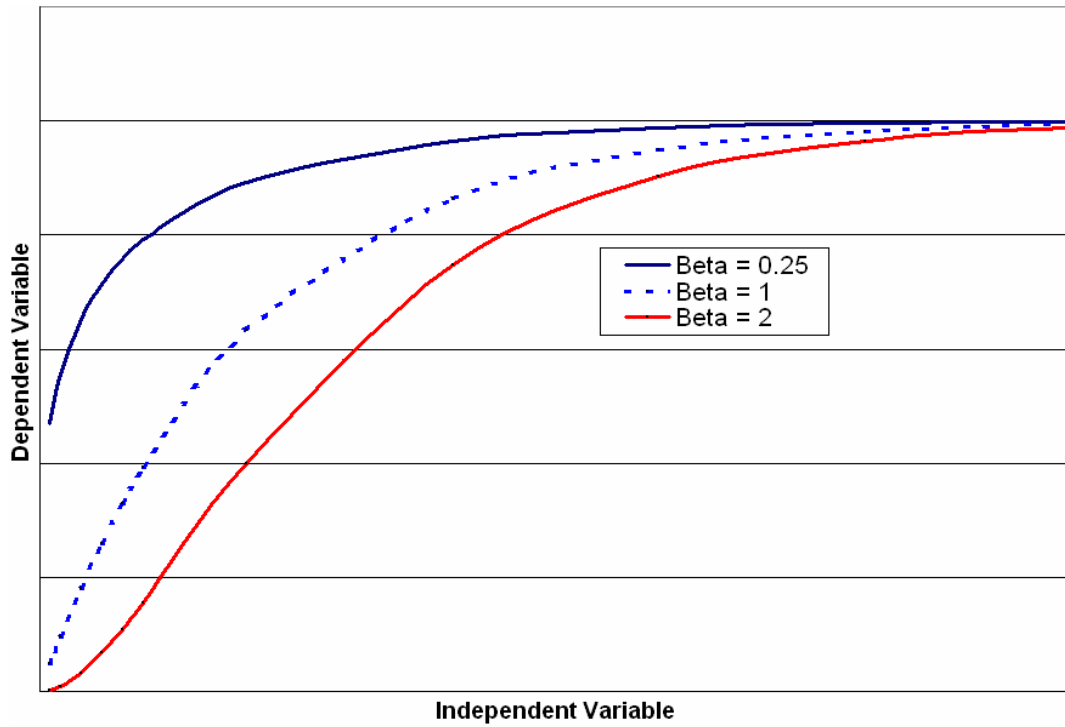
Fig. 7 — Alpha held constant at 0.5 while changing beta.
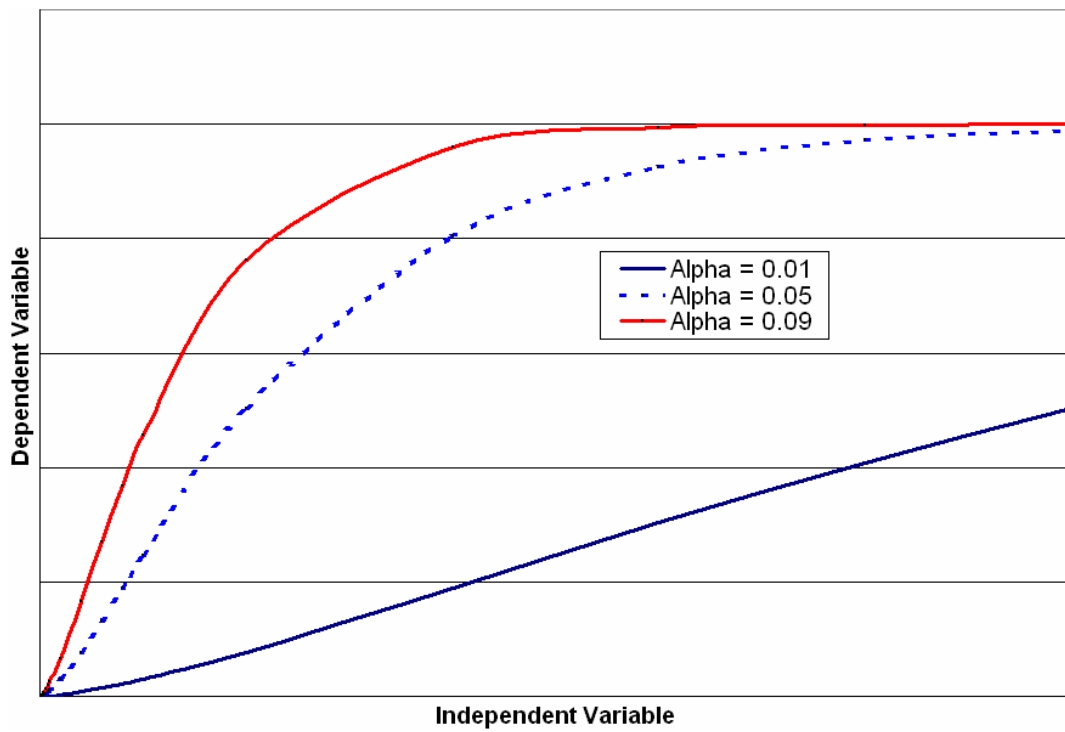
Fig. 8 — Beta held constant at 1.5 while changing alpha.

When transposing the predicted YP, obtained from the generalized rheological model, over the measured YP from the bench top blender data, **Fig. 9** was obtained. **Fig. 10** offers a comparison of the predicted YP and blender YP. Notice that the degree of accuracy in terms of R^2 is approximately 0.87.
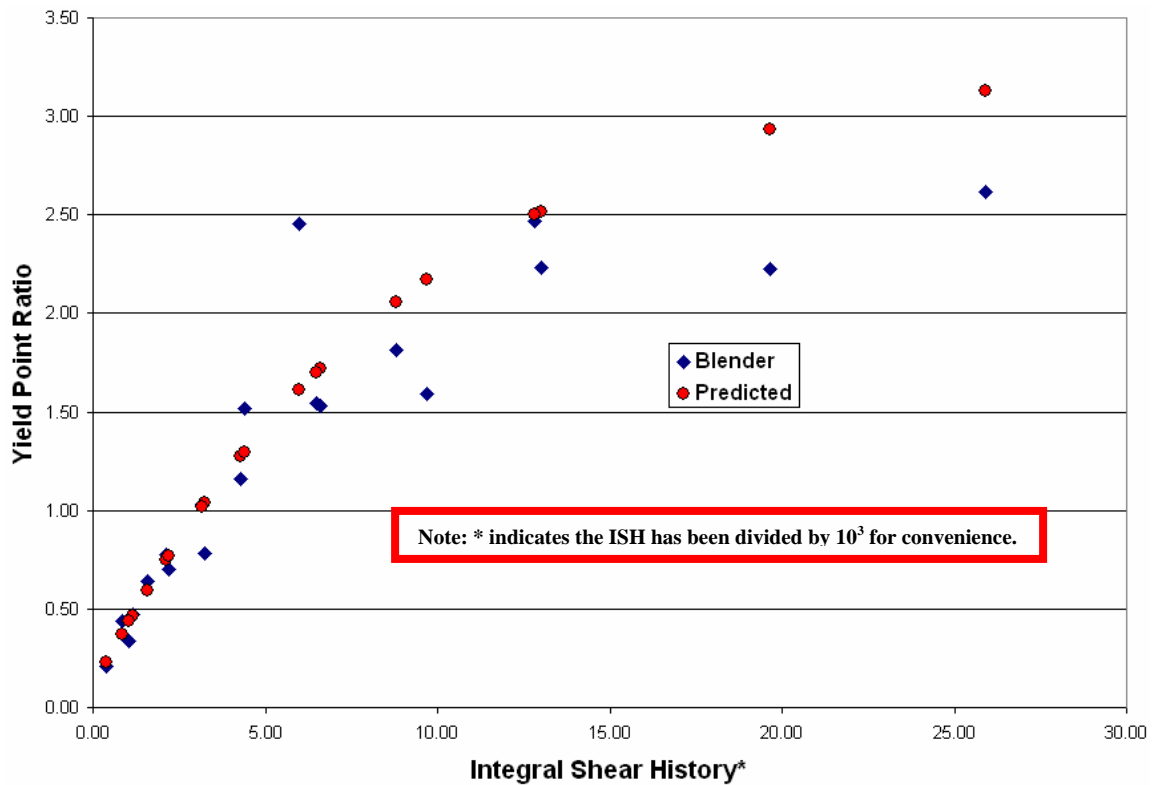
Fig. 9 — Fluid System A – prediction of bench top yield point using rheological model.

Note: The data point circled in red does not follow the normal trend of the rest of the data. It has been retested several times with the same result. The reason for this behavior is unknown.

y = 1.0728x
$R^2 = 0.8726$
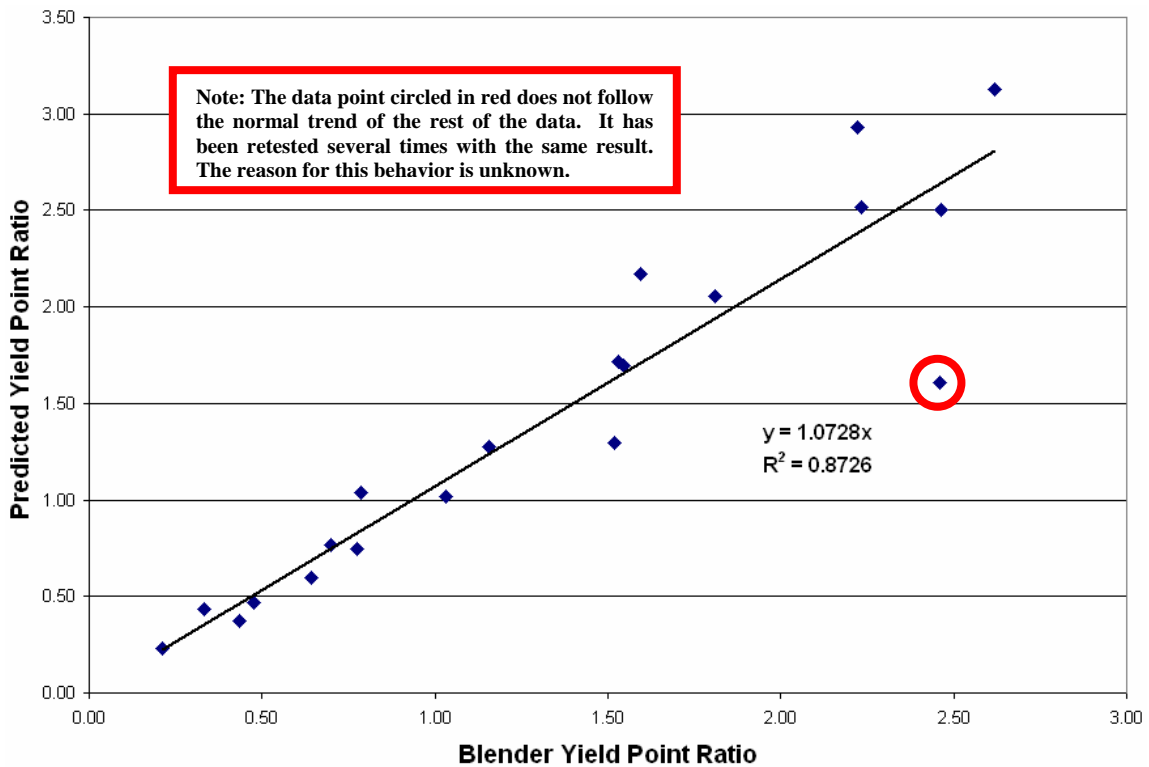
Fig. 10 — Fluid System A – predicted and blender YP comparison.

4.4 Scaled Model Tests

The scaled model was designed using similitude, a proven modeling strategy in many engineering applications. Specifically, Buckingham's Pi Theorem was implemented to derive dimensionless terms that could characterize different geometrical parameters that would allow the scaled model to accurately predict actual wellbore conditions. Buckingham's Pi Theorem states that, "the number of dimensionless and independent quantities required to express a relationship among variables in any phenomenon is equal to the number of quantities involved minus the number of dimensions."[35] Typically, there are three dimensions, mass (M), length (L), and time (t),

in every modeling situation. Buckingham's Pi Theorem can best be described in the following example.

Consider flow of a Newtonian fluid in a pipe. The variables that characterize the flow are pipe diameter, density, velocity, viscosity, pipe roughness, pipe length, and pressure drop. In this analysis, there are six independent terms and one dependent term. Specifically, conventional modeling implies that pressure drop is a function of the other six variables as shown in Eq. 5.

$$\Delta P = f(D, \rho, V, \mu, \varepsilon, L) \quad \dots\dots\dots\dots\dots\dots\dots\dots\dots\dots\dots\dots\dots (5)$$

Using similitude, the number of dimensionless terms, according to Buckingham's Pi Theorem, is four hence reducing testing and development cost by 40% - 60%.

i.e. Number of Quantities (7) – Number of Dimensions (3) = Dimensionless Terms (4)

A generalized product solution form of Buckingham's Pi Theorem can be expressed as:

$$\pi_1 = f(\pi_2, \pi_3, \pi_4 \dots) = A(\pi_2)^{B_1} (\pi_3)^{B_2} (\pi_4)^{B_3} \quad \dots\dots\dots\dots\dots\dots\dots\dots\dots (6)$$

Applying this strategy to the flow of a Newtonian fluid in a pipe yields Eq. 7.

$$\left[\frac{\Delta P}{\left(\frac{\rho V^2}{2}\right)}\right] = 64\left[\frac{\rho V D}{\mu}\right]^{-1}\left[\frac{L}{D}\right]^{-1} f(\varepsilon) \quad \dots\dots\dots\dots\dots\dots\dots\dots (7)$$

It is apparent that using similitude results in dimensionless terms that correspond to the Moody Friction Chart for pipe flow. The left hand side of the equation is the friction

factor, and the terms in order from left to right on the right side of the equation are Reynolds Number, equivalent pipe length, and pipe roughness.

The dimensionless terms listed in **Fig. 11** for the scaled model were derived using the same methodology presented in the pipe flow example.

$$\frac{\rho_M V_M (D_W - D_B)}{\mu_{\infty M}} \rightarrow N_{ReM} \qquad \frac{D_N}{D_W} \rightarrow Geometrical\ Ratio$$

$$\frac{\rho_{PLIP} V_{PLIP} D_N}{\mu_{\infty PLIP}} \rightarrow N_{RePLIP} \qquad \frac{D_B}{D_W} \rightarrow Geometrical\ Ratio$$

$$\frac{\rho_M \tau_{oM} D_W^2}{\mu_{\infty M}^2} \rightarrow N_{HeM} \qquad \frac{\tau_{oM}}{\tau_{oPLIP}} \rightarrow Rheological\ Ratio$$

$$\frac{\rho_{PLIP} \tau_{oPLIP} D_N^2}{\mu_{\infty PLIP}^2} \rightarrow N_{RePLIP} \qquad \frac{\rho_M}{\rho_{PLIP}} \rightarrow Rheological\ Ratio$$

$$\frac{\rho_{PLIP} V_{PLIP}^2}{2\tau_{oPLIP}} \rightarrow PMN$$

Fig. 11 — Similitude terms.

All of the scaling terms either have a geometrical or rheological meaning to both the full scale and model systems. Usually, in a modeling scheme, there is at least one term that is the core of the analysis. In this case, the most important term, Pi Mixing Number (PMN), shown at the bottom of Fig. 11, has a significant influence on the data analysis. **Fig. 12** shows a snap shot of the complex spreadsheet used to design the scaled model.

Inputs

Variable	Full Scale	Model	Units
D_B	9.6	2.500	in
D_N	0.5	0.200	in
D_W	12.6	3.000	in
$\mu_{\infty PLIP}$	68.0	68.0	cp
$\mu_{\infty M}$	83.0	83.0	cp
N	3.0	3.0	none
ρ_{PLIP}	9.3	9.3	ppg
ρ_M	13.0	13.0	ppg
τ_{PLIP}	40.0	40.0	lb/100ft²
τ_M	35.0	35.0	lb/100ft²
V_{PLIP}	68.1	68.1	ft/s
V_M	5.8	32.7	ft/s
Q_M	0.3	0.045	ft³/s
Q_{PLIP}	0.3	0.045	ft³/s
Q_M	125.0	20.0	gal/min
Q_{PLIP}	125.0	20.0	gal/min

NOTE: Assumes $Q_M = Q_{PLIP}$ at all times

Drillstring OD = (Full Scale D_B/Model D_B) * 2.875	0.747	in

Dimensionless Groups

Group	Full Scale	Model	Units
Reynolds Number			
Mud	2,487	2,367	none
PLIP	4,307	1,723	none
Hedstrom Number			
Mud	387,760	21,982	none
PLIP	743.8	119.0	none
Pi – Mixing Number	12.49	12.49	Key Pi Term
Ratio of D_N to D_W	0.04	0.07	none
Ratio of D_B to D_W	0.76	0.83	none
Ratio of t_M to t_{PLIP}	0.88	0.88	none
Ratio of ρ_M to ρ_{PLIP}	1.40	1.40	none
Number of Nozzles	3.00	3.00	none

Note: Ratio of D_N to D_W is of minimal importance

Fig. 12 — Scaled model design spreadsheet.

The left side of the spreadsheet is used to input both geometrical and rheological data. Notice that the green represents full scale data, and the light blue corresponds to the model data. The right side of the spreadsheet contains the dimensionless terms. Indicated in the red box with white lettering is the PMN.

Fig. 13 explains the methodology for developing the similitude spreadsheet.

---

1. Input all full scale data.
2. Choose model dimensions that allow the dimensionless terms for the full scale and model to become as close as possible.

Note/Warning: DO NOT Compromise fluid properties between full scale and pilot model.

Fig. 13 — Similitude procedure.

The only scaling factors that could not be designed according to the similitude approach were the distance from the surface to the drill bit, the distance from the drill bit to the thief zones, and the size of the thief ports. In real life situations, the exact size and location of the fracture is not known.   Therefore, when using PLIP to treat lost circulation, the drill bit is raised to the last casing shoe depth, and the treatment is placed with respect to the volume of drilling fluid lost per hour.

For the scaled model, the distance from the surface to the drill bit was obtained by Eq. 8, and the distance from the drill bit to the thief zones was given by Eq. 9. These distances were chosen according to industry accepted pipe flow rules of thumb.[36]   In addition, the sizes of the thief ports were varied in increments of ½ in. However, the results of the project were consistent in all cases.

$$L_{SD} = 20D \dotfill (8)$$

$$L_{DT} = 10D \dotfill (9)$$

In the similitude analysis, all of the dimensionless terms except Reynolds Number and Hedstrom Number were matched exactly. Therefore, an investigation on the physical meanings of these non-equal parameters was essential.

According to conventional pipe flow characteristics, turbulent flow occurs at a Reynolds Number of $\geq 2,100$ in most cases. As can be seen from Fig. 12, all of the pipe flow except for in the model drill string operates in the turbulent regime. However, since the flow in the model is nearly turbulent, and the flow in actual conditions is

guaranteed to be turbulent, then the reacted product from the model will present a comparable YP to actual treatment conditions.

Correlations, like that of **Fig. 14**, have been developed between Hedstrom Number and critical values (C_c) from the Bingham plastic model that explain the difficulty of achieving turbulent flow. Since all pipe flow is turbulent except for in the model drill string, then the Hedstrom Number for that location in the model and actual conditions must be compared. Fig. 14 indicates that the difficulty in developing turbulent flow in both conditions is minimal; therefore, the comparison shows that Hedstrom Number for this condition is insignificant.[37]
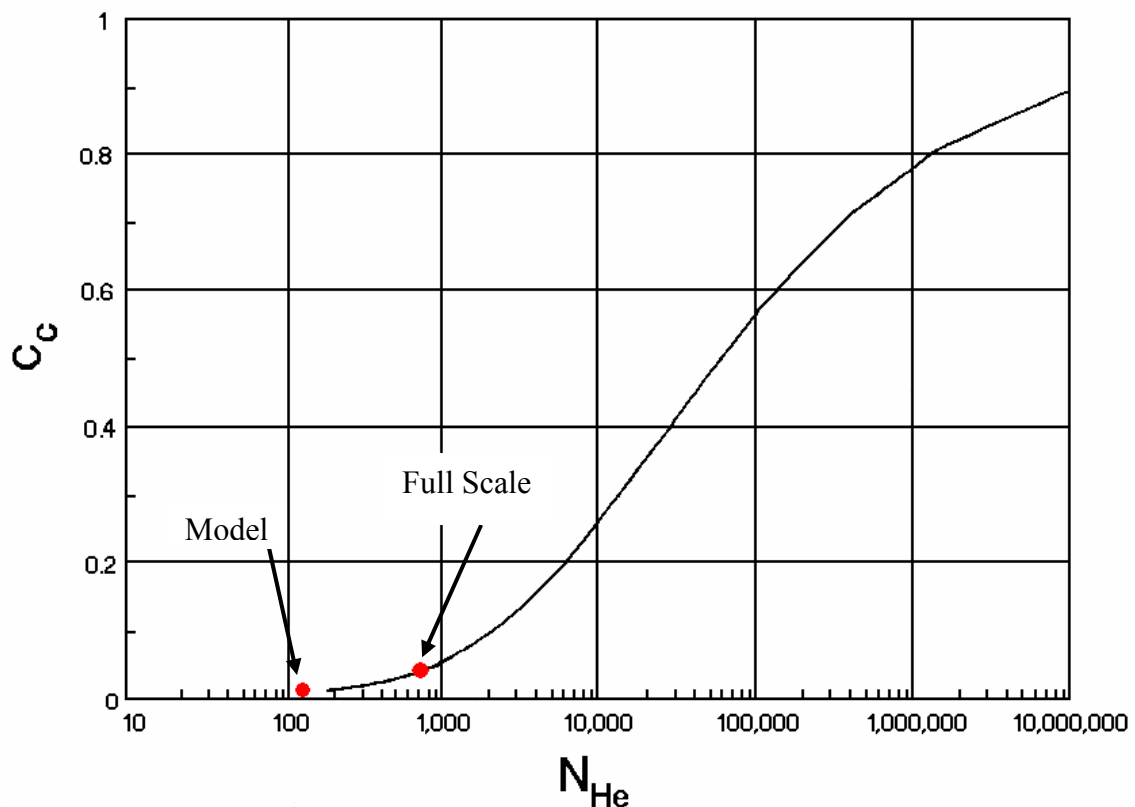
Fig. 14 — C_c - Hedstrom number correlation, (Steffe, 1996).

4.4.1 Apparatus

The model test apparatus was equipped with two pumps that classify the two-stream lost circulation treatment as dual flow. The PLIP was pumped through the drill string, and the mud was pumped down the annulus. In the lower left corner of **Fig. 15**, a picture of the drill bit spray can be seen. In addition, the model was affixed with a thief zone, and relief valves. The thief zone was present to allow for sample collection, and the relief valves ensured that the model did not over pressure. Also, a stabilizer was mounted just above the drill bit to ensure that the drill string assembly remained centralized within the wellbore.
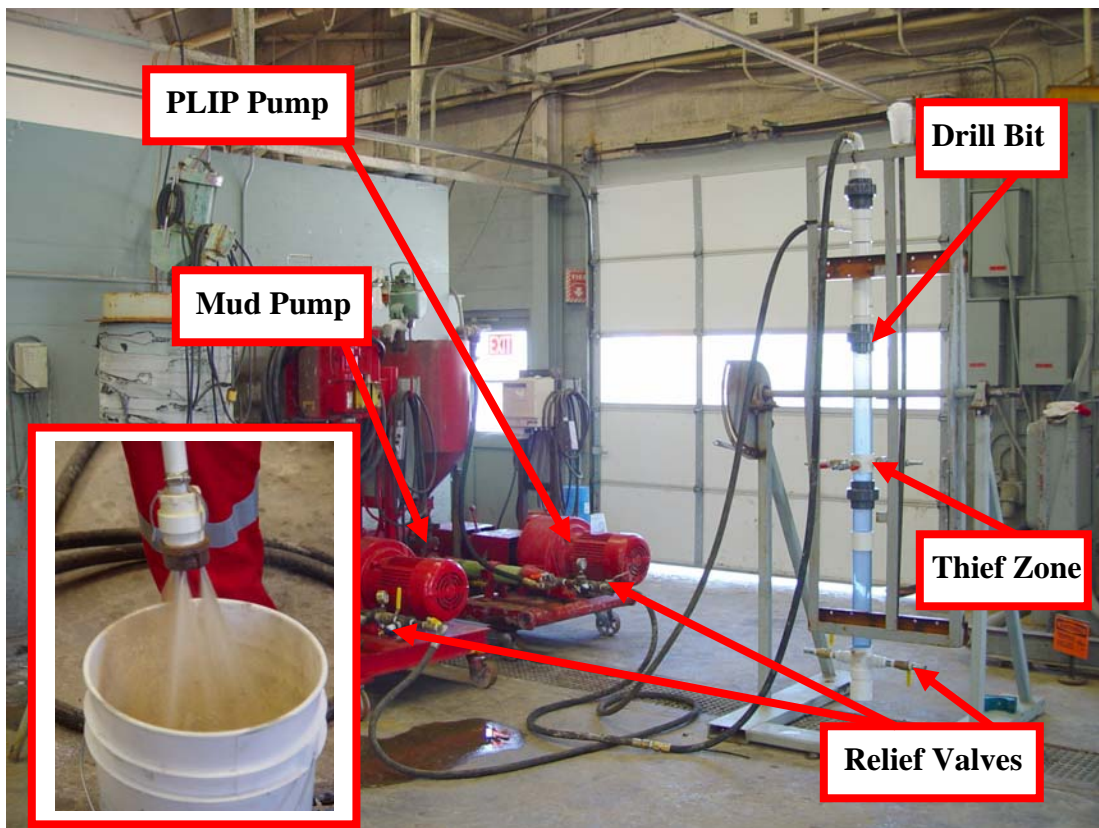
Fig. 15 — Scaled model test apparatus.

4.4.2 Procedure

1. Fill the model wellbore with drilling fluid to best simulate actual conditions.

2. Simultaneously begin flowing mud and PLIP at the same flow rate.

3. Allow flow through thief zones until adequate sample is collected.

4. Measure the YP of the sample at 30 min curing time.

The test matrix used for this procedure called for flow rates ranging from 5 to 20 gal/min under two conditions. One condition utilized the use of a screen placed in the mouth of the thief ports, while the other condition removed the screen and flowed through open ports. By placing the screen in the path of the reacted product, additional shear influenced the quality (YP) of the sample. Also, by introducing more shear to the system, the hypothesis of accumulated shear could be proven. Therefore, a best case and worst case scenario was created for downhole mixing.

4.4.3 Data Analysis

As in the blender experiments, the data for the model tests were analyzed using the theory of integral shear history. Eq. 10 explains how the ISH for each of the described pilot conditions was calculated.

$$\text{ISH} = \dot{\gamma}^P_{Bit} \Delta t_{Bit} + \dot{\gamma}^P_{Annulus} \Delta t_{Annulus} + \dot{\gamma}^P_{Thief} \Delta t_{Thief} + \dot{\gamma}^P_{Screen} \Delta t_{Screen} \quad \text{.........................} (10)$$

In Eq. 10, p represents the materials sensitivity to shear, Δt_x represents the effective time of mixing in a particular area of the pilot model, and γ is the shear rate of the area in the model in question. Since Δt_x is unknown for any area of the scale model,

then it was determined by iteration. The shear rate in each of the sections can be calculated from Eq. 11.

$$\dot{\gamma} = \frac{4\dot{Q}}{\pi R^3}$$ .... (11)

As can be seen, shear rate is a function of flow rate and section radius.

Fig. 16 is a graphical representation of the YP achieved at each of the tested flow rates in both the screened and no-screen cases for the wellbore model. This plot proves that the hypothesis of increasing YP with increasing ISH is correct. At every chosen flow rate the YP is greater in the screened cases than in the no-screen cases.
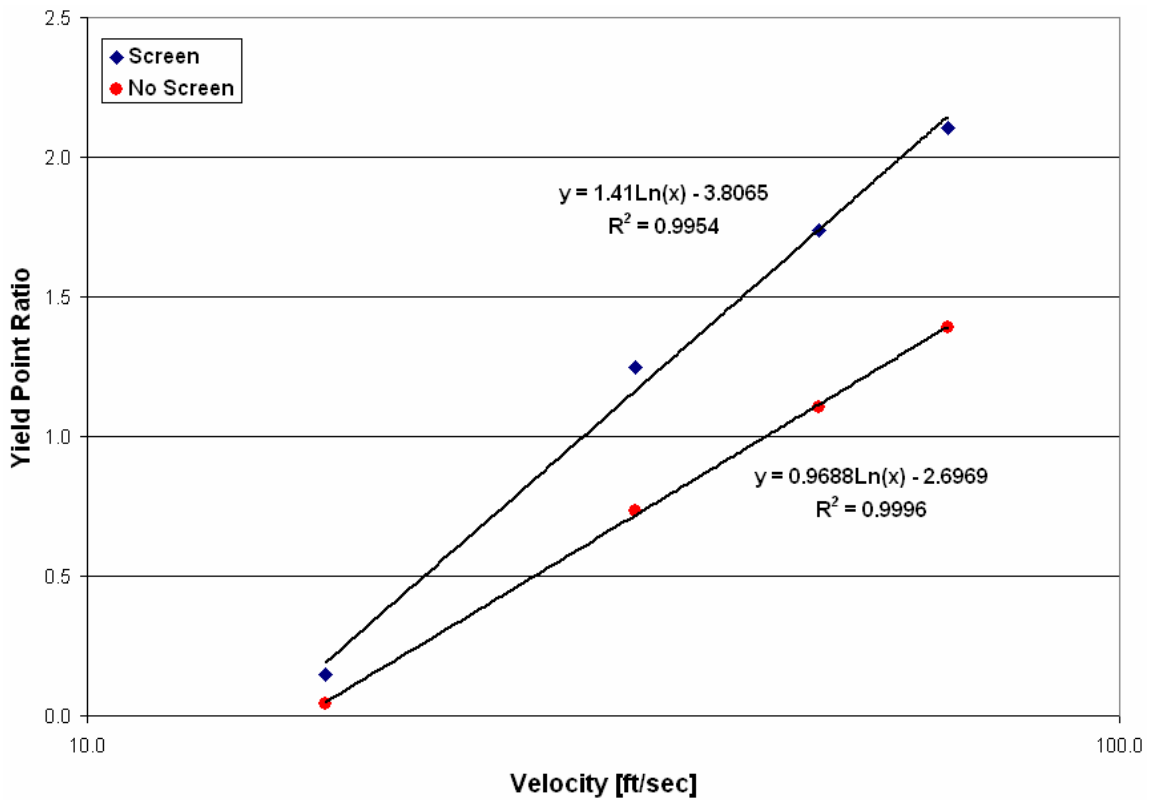
Fig. 16 — Fluid System A – pilot scale increase in YP with increasing nozzle velocity.

Furthermore, it can be seen from **Fig. 17** that ISH controls the quality of the product. It seems that there is a specific YP for a specific ISH. However, the YP will vary with every combination of fluid properties.
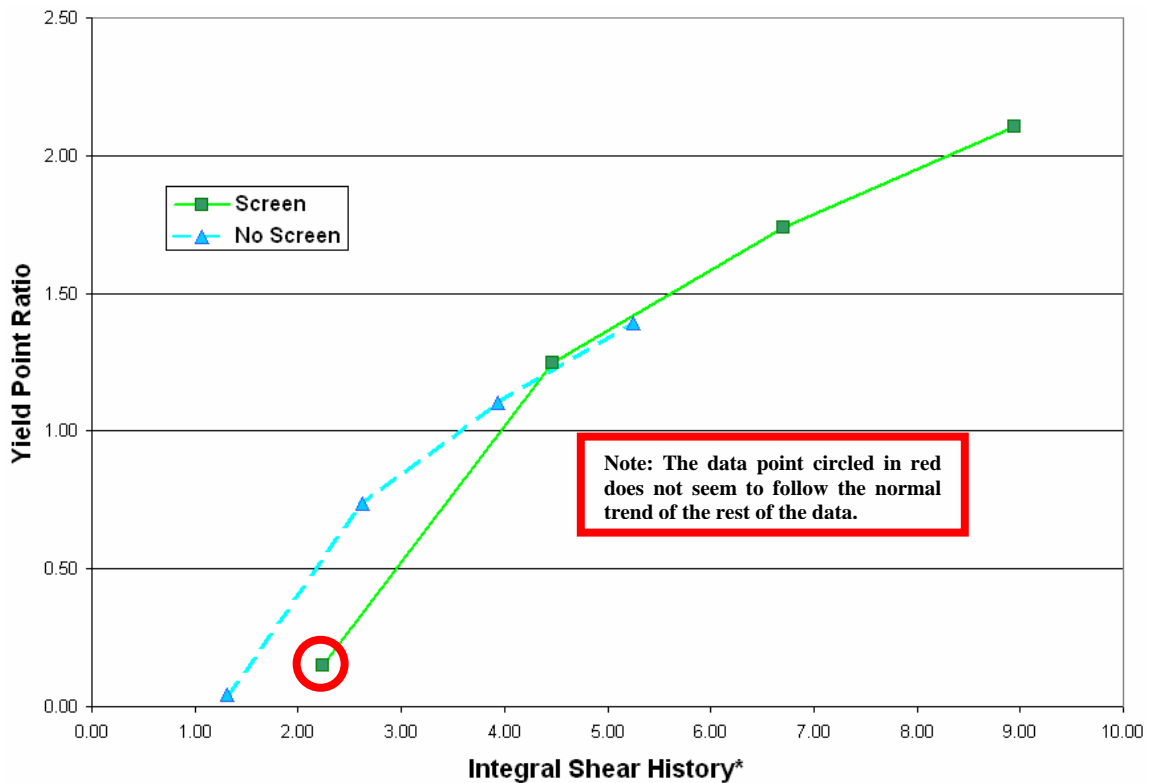
Fig. 17 — Fluid System A – effect of ISH on YP in the pilot model.

In addition, **Fig. 18** shows the predicted YP representation for the pilot model tests. With the exception of the low YP data circled in red, the generalized rheological model is an accurate interpretation of the two-stream jet mixing.
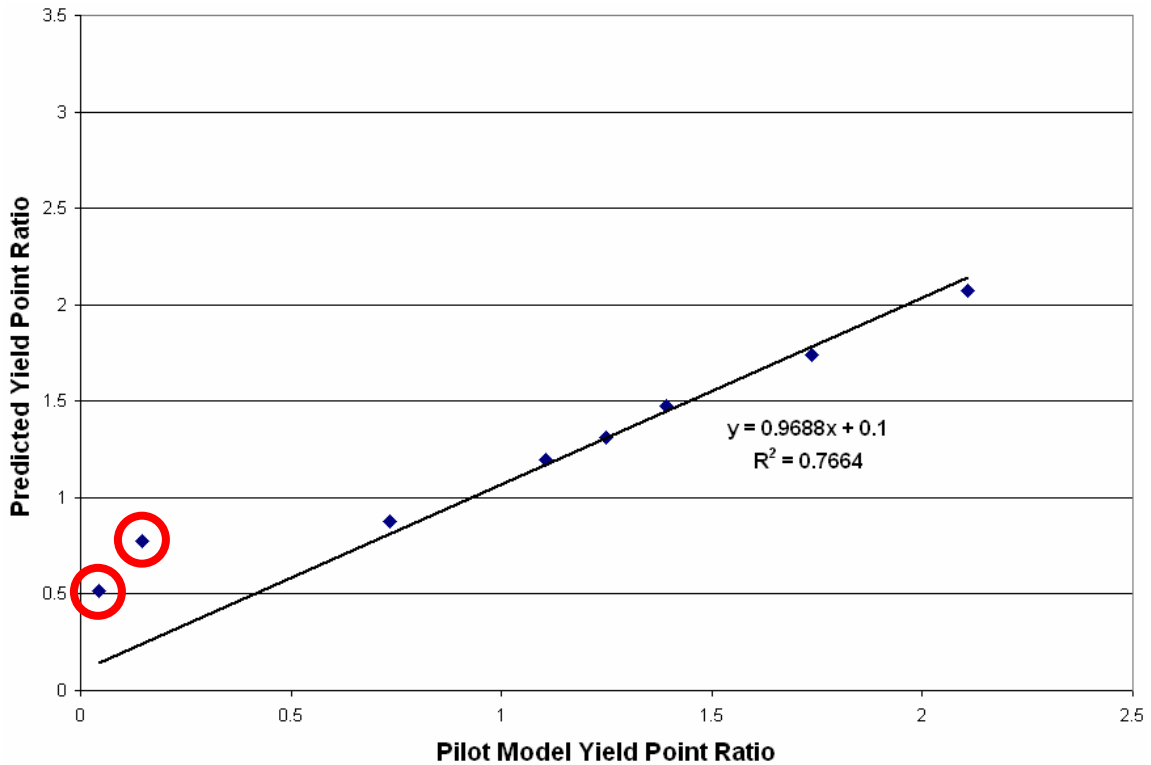
Fig. 18 — Fluid System A – predicted and pilot model YP comparison.

4.5 Correlation

By overlaying Fig. 9 and Fig. 17 (shown in **Fig. 19**), it is shown that the pilot model is an accurate illustration of the bench top blender tests. Also, ISH seems to be an accurate representation of the degree of mixing required to obtain a desired YP. Remember that part of the goal is to simulate downhole mixing using mechanical agitation. The methodology described in this thesis does just that.
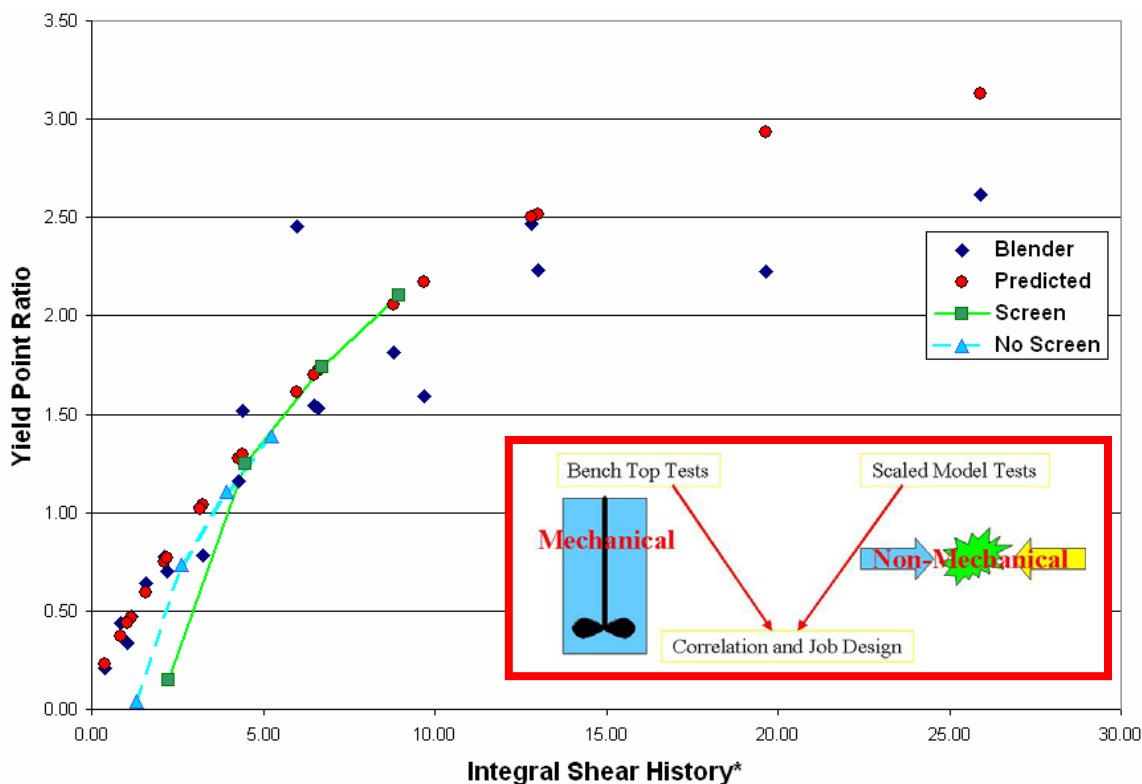
Fig. 19 — Fluid System A – effect of ISH on YP during all tests.

As stated earlier, the PMN becomes important in designing downhole PLIP treatments. It turns out that PMN is highly correlated with ISH and is key to relating lab mechanical mixing to fluid-to-fluid in-situ downhole mixing. Since the pilot data depicts the predicted data to a high degree of accuracy, then it can be assumed that the PMN for both cases is the same at a particular YP. **Fig. 20** shows the ISH* – PMN correlation.
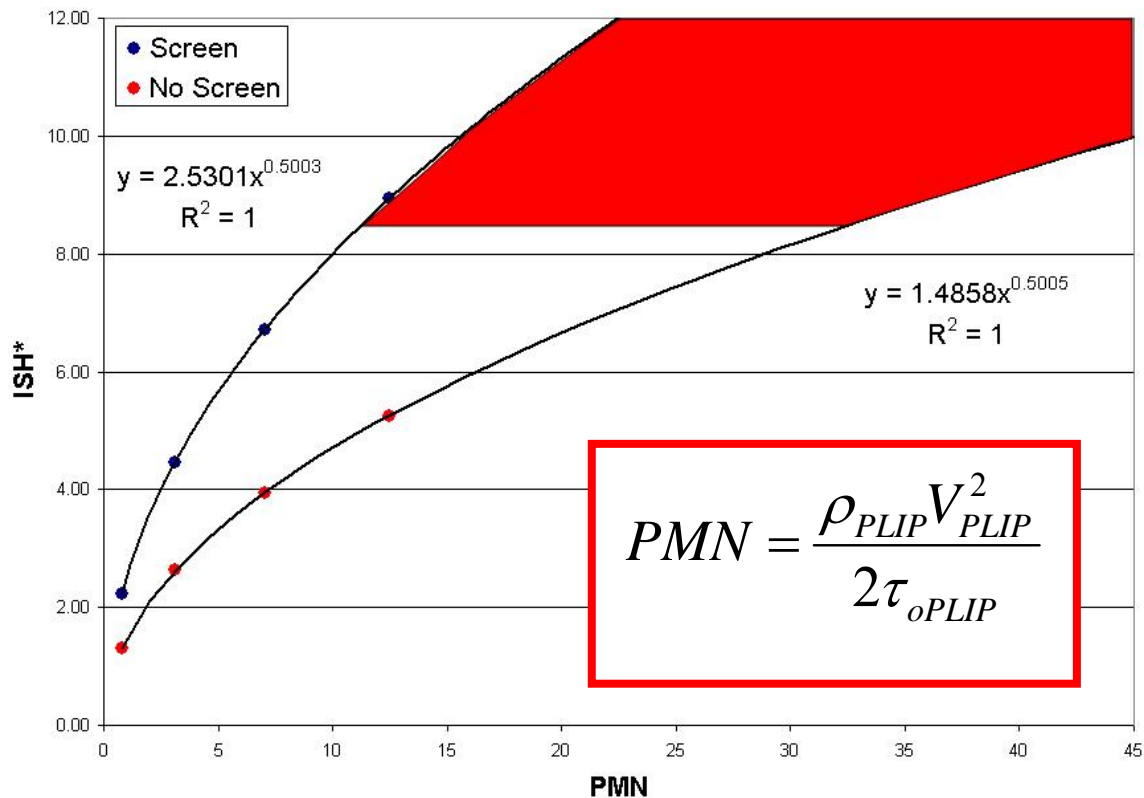
Fig. 20 — Fluid System A – ISH- PMN correlation.

In the similitude spreadsheet (Fig. 12), values can be changed that yield different PMN values. Specifically, the flow rate of the PLIP was changed according to the flow rates obtained in the pilot model. Since the ISH is known, and now the PMN is known for a given flow rate in the pilot scale, then Fig. 20 can be obtained, encompassing a best case scenario (screen) and worst case scenario (no screen).

4.5.1 Understanding the Analysis

The analysis and job design strategy can be best understood using the following example. **Fig 21** shows how to determine the PMN range for a particular YP.
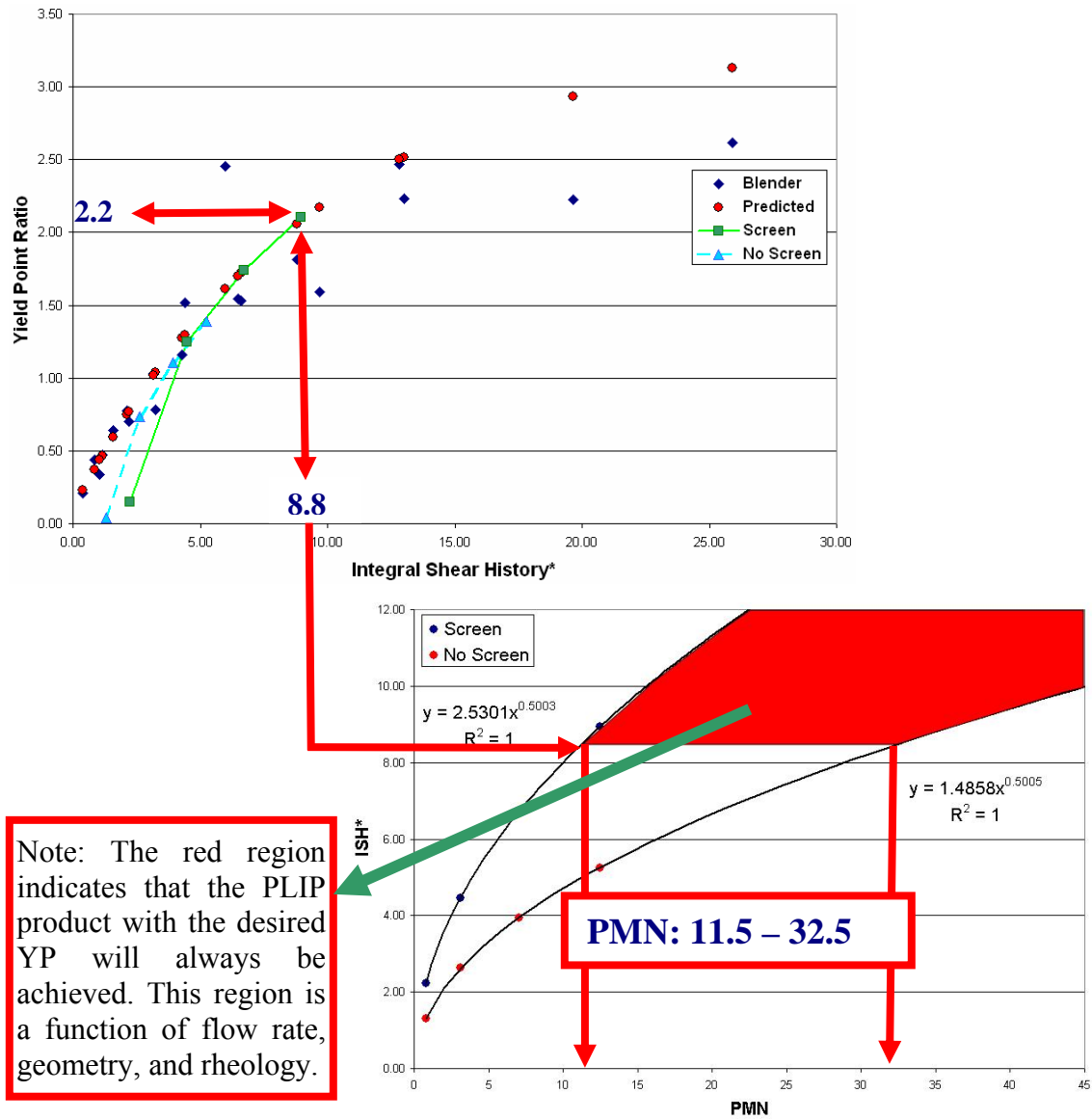
Fig. 21 — PMN determination.

First, the desired YP must be selected. For purposes of this example, the desired YP is 2,000 Pa. Second, read the ISH* that corresponds to the YP. Third, follow the ISH* along the ISH* – PMN correlation to obtain a window of PMN's. Finally, use **Fig. 22** to obtain a range of PLIP placement flow rates. Again, a worst case and best case scenario is presented. The higher flow rate assumes that the only shear that is presented to the system is due to jet mixing at the bit; whereas, the lower flow rate assumes that other sources of shear are present downhole (e.g. fracture entrance effects).

$$\dot{Q} = 2.9 - 4.8\,[\text{bbl/min}] = \dot{Q}_{FP} = \dot{Q}_M$$

$y = 35.601x^{0.4973}$

$R^2 = 1$
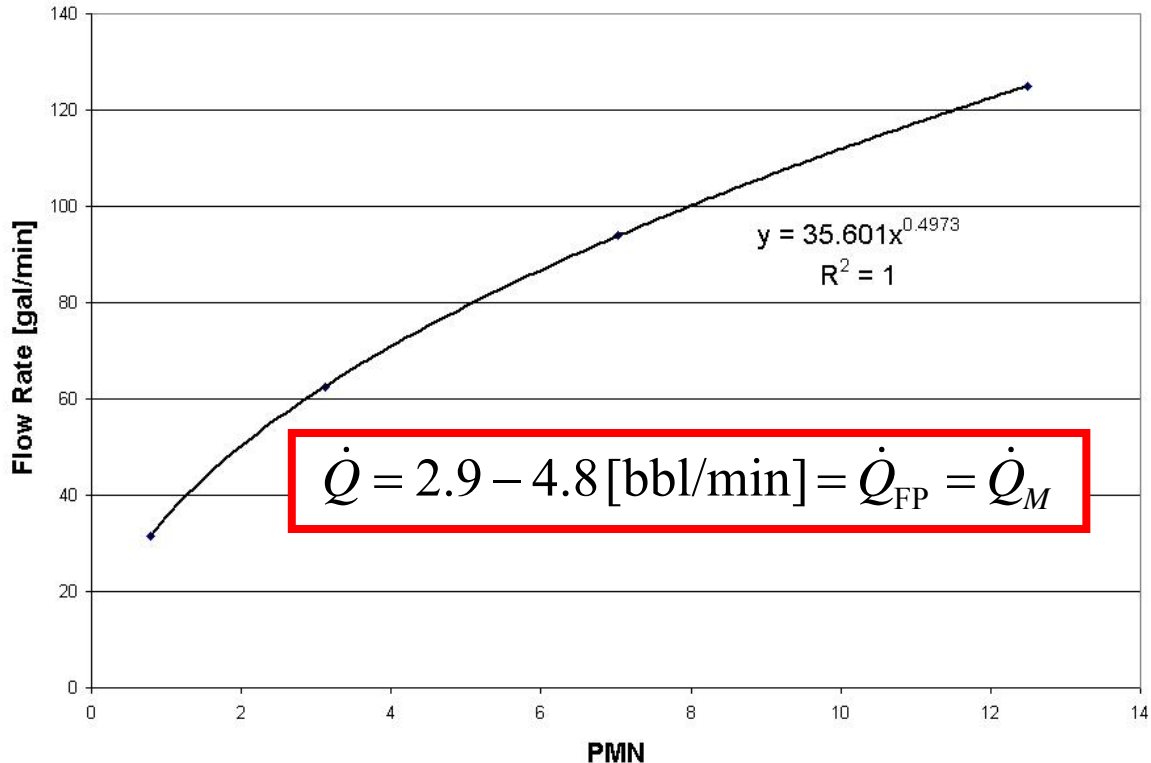
Fig. 22 — Flow rate - PMN correlation.

4.6 Additional Information

The data analysis indicates that the product quality greatly depends on α, β, and *p*. **Table 3** shows these values for the three Halliburton drilling fluids tested.

Table 3 — Drilling Fluid Constants

Mud Type	p	Alpha	Beta
Fluid System A	1	0.000105	1
Fluid System B	1.11	0.00005	1.5
Fluid System C	1.2	0.000006	0.2

Notice that the drilling fluids are highly sensitive to these values. Particularly, α and β can be used to determine the best fluids for a severe lost circulation treatment. **Fig. 23** offers a map of acceptable parameters that correspond to adequate downhole mixing of any two-stream lost circulation treatment.
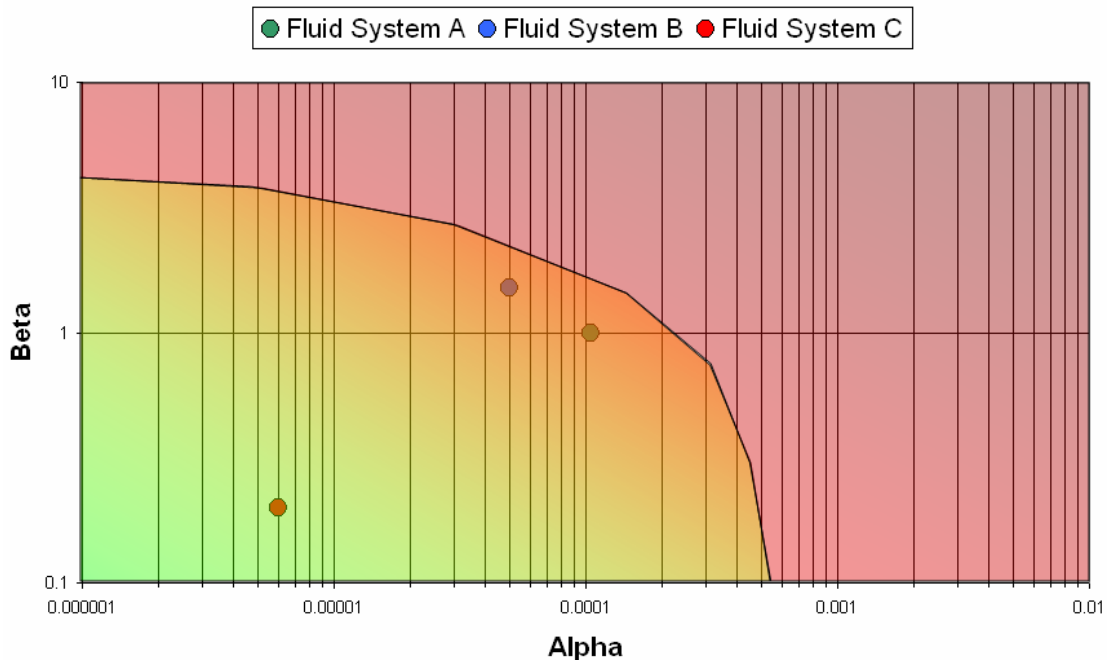
Fig. 23 — Mixing sensitivity index.

The dashed line in Fig. 23 indicates the suspected crossover region between a reacted product (RP) with a yield point of 2000 lb/100ft^2 or greater (lower left region) versus a product with a yield point less than 2000 lb/100ft^2 (upper right region). It can be observed that Fluid System C provides a higher YP at a relatively lower mixing energy compared to the other two mud systems. The other two drilling fluids also offer a high YP, but they require more mixing energy to achieve this same consistency.

CHAPTER V

SUMMARY, CONCLUSIONS, AND FUTURE WORK RECOMMENDATIONS

5.1 Summary

One of the most cumbersome problems associated with drilling unconventional reservoirs and depleted zones is lost circulation. Many times losses encountered while drilling challenging formations occur from fracture propagation.

Recently, literature has been published that suggest the best way to combat fracture thief zones is to place LCM's in the fracture while simultaneously widening the fracture. This process increases the fracture closure stress, thus building wellbore integrity and widening the mud weight window.

The most recent advancements in LCM's that achieve the goal of building wellbore strength require adequate downhole mixing of two-stream systems. Therefore, an in-depth analysis of actual downhole mixing capabilities is an essential step ahead while striving toward a 100% success rate for two-stream LCM placements. This research effort was geared toward developing best practice LCM placement flow rates for Halliburton's DrillAhead® product, PLIP.

5.2 Conclusions

It was found that an envelope of optimal flow rates can be achieved using data from the scaled pilot model and the laboratory experiments. By using the product's high sensitivity to shear, a correlation can be determined that depends on wellbore geometry, fluid properties, and flow rate for treatment design.

In addition, it was discovered that each drilling fluid behaves differently when subjected to the same formulation of PLIP. By using these unique behaviors, a Mixing Sensitivity Index (MSI) can be developed that allows for proper drilling fluid design in case of lost circulation.

5.3 Future Work Recommendations

To better simulate actual downhole conditions, a model that incorporates the High Temperatures and High Pressures (HTHP) of reservoirs could be developed. It is understood that when the PLIP product is subjected to HTHP, it presents higher YP's at shorter curing times in the reacted state.

In addition, a similar analysis used to obtain the downhole Plastic Viscosity (PV) would be beneficial. By measuring the YP for the product, the pressure required to dislodge the reacted product from a fracture is now known. If the PV can be understood in the same manner, then the distance that the product flows down the fracture will then be established.

Finally, further experiments can be conducted on all LCM's that require two-stream mixing to better define the MSI. Once an accurate MSI is developed, then the best LCM's to combat fracture propagation lost circulation will be determined.

NOMENCLATURE

A = plastic viscosity parameter, dimensionless

a = scaling exponent, dimensionless

A_{CS} = cross sectional Area, ft^2

A_W = wellbore area, ft^2

B = plastic viscosity parameter, dimensionless

b = scaling exponent, dimensionless

$B - P$ = blender – predicted

c = scaling exponent, dimensionless

D = pipe diameter, in

D_B = diameter of drill bit, in

D_N = diameter of nozzles, in

D_W = diameter of wellbore, in

FCS = fracture closure stress, psi

$HTHP$ = high temperature - high pressure

$ISH*$ = integral shear history, dimensionless

j = number of independent quantities, dimensionless

k = number of dimensionless terms, dimensionless

K_1 = shear rate constant, dimensionless

L = length, ft

LCM = lost circulation material

L_{SD} = distance from surface to drill bit, in

L_{DT} = distance from drill bit to thief ports, in

M = mass, lb

MSI = mixing sensitivity index

MYPD = manual yield point device

n = number of dimensions, dimensionless

N = number of nozzles, dimensionless

N_{He} = Hedstrom number, dimensionless

N_{Re} = Reynolds number, dimensionless

p = material property based on sensitivity to shear, dimensionless

PMN = pi mixing number, dimensionless

PV = plastic viscosity, cp

P_W = wedded perimeter, in

Q = flow rate, gal/min

R = radius, in

R_H = hydraulic radius, in

RPM = revolutions per minute, rpm

t = time, sec

t_{mix} = mixing time, sec

V = fluid velocity, ft/sec

YP = yield point, lb/100ft^2

YP_0 = initial yield point, lb/100ft^2

YP_∞ = terminal yield point, lb/100ft^2

α = pseudo rate constant, dimensionless

β = material reaction parameter, dimensionless

ΔP = pressure differential, psi

$\Delta t_{Annulus}$ = effective shearing time in annulus, sec

Δt_{Bit} = effective shearing time immediately below drill bit, sec

Δt_{Screen} = effective shearing time of screen, sec

Δt_{Thief} = effective shearing time in thief port, sec

ε = pipe roughness, dimensionless

γ = shear rate, 1/sec

μ = viscosity, cp

μ_{∞} = plastic viscosity, cp

ρ = fluid density, lb/gal

τ_o = yield point, lb/100ft^2

Subscripts

M = mud

PLIP = product based on latex inversion process

RP = reacted product

REFERENCES

1. Shryock, S. H.: "Geothermal Well Cementing Technology," paper SPE 12454 presented at the 1984 SPE Annual Offshore Technology Conference, Singapore, 21-24 February.

2. Davies, D. R. and Hartog, J. J.: "Foamed Cement – A Cement with Many Applications," paper SPE 9598 presented at the 1981 SPE Middle East Oil Technical Conference, Manama, Bahrain, 9-12 March.

3. Nayberg, T. M. and Petty, B. R.: "Laboratory Study of Lost Circulation Materials for Use in Oil-Base Drilling Muds," paper SPE 14995 presented at the 1986 SPE Deep Drilling and Production Symposium, Amarillo, Texas, 6-8 April.

4. Nayberg, T. M.: "Laboratory Study of Lost Circulation Materials for Use in Both Oil-Based and Water-Based Drilling Muds," paper SPE 14723 presented at the 1986 IADC/SPE Drilling Conference, Dallas, Texas, 10-12 February.

5. Adachi, J., Bailey, L., Houwen, O. H., Meeten, G. H., and Way, P. W.: "Depleted Zone Drilling: Reducing Mud Losses Into Fractures," paper IADC/SPE 87224 presented at the 2004 IADC/SPE Drilling Conference, Dallas, Texas, 2-4 March.

6. Messenger, T. U.: *Lost Circulation*. Penn Well Publishing Co., Tulsa, OK (1981).

7. Dupriest, F. E.: "Fracture Closure Stress (FCS) and Lost Returns Practices," paper SPE/IADC 92192 selected for presentation at the 2005 SPE/IADC Drilling Conference, Amsterdam, The Netherlands, 23-25 February.

8. Fidan, E., Babadagli, T., and Kuru, E.: "Use of Cement As Lost Circulation Material – Field Case Studies," paper IADC/SPE 88005 presented at the 2004 IADC/SPE Asia Pacific Drilling Technology Conference and Exhibition, Kuala Lumpur, Malaysia, 13-15 September.

9. Ali, A., Kalloo, C. L., and Singh, U. B.: "A Practical Approach for Preventing Lost Circulation in Severely Depleted Unconsolidated Sandstone Reservoirs," paper SPE/IADC 21917 presented at the 1991 SPE/IADC Drilling Conference, Amsterdam, The Netherlands, 11-14 March.

10. Economides, M. J., Watters, L. T., and Dunn-Norman, S.: *Petroleum Well Construction*. Chapter 5. John Wiley and Sons, New York (1998) 135.

11. Clark, C. O., Haskin, C. A., and Hull, T.R.: "Chemical Method for Formation Plugging," *Journal of Petroleum Technology* (May 1971) **23**, 559.

12. White, R. J.: "Lost Circulation Materials and Their Evaluation," *API Drilling and Production Practices* (1956) **23**, 352.

13. Whitfill, D. L. and Hemphill, T.: "All Lost-Circulation Materials and Systems Are Not Created Equal," paper SPE 84319 presented at the 2003 SPE Annual Technical Conference and Exhibition, Denver, Colorado, 5-8 October.

14. Loeppke, G. E., Glowka, D. A., and Wright, E. K.: "Design and Evaluation of Lost-Circulation Materials for Severe Environments," paper SPE 18022 presented at the 1988 SPE Annual Technical Conference and Exhibition, Houston, Texas, 2-5 October.

15. Fuh, G., Morita, N., Boyd, P. A., and McGoffin, S. J.: "A New Approach to Preventing Lost Circulation While Drilling," paper SPE 24599 presented at the 1992 SPE Annual Technical Conference and Exhibition, Washington, DC, 4-7 October.

16. Nahm, J. J., Romero, R. N., Wyant, R. E., Hale, A. A., Briggs, B. R., Smith, T. R., Lombardi, M. A., and Keedy, C. R.: "Universal Fluid: A Drilling Fluid to Reduce Lost Circulation and Improve Cementing," paper IADC/SPE 27448 presented at the 1994 IADC/SPE Drilling Conference, Dallas, Texas, 15-18 February.

17. Alleman, J., Owen, B., Cornay, F., and Weintritt, D. J.: "Multi-functional Solid Lubricant Reduces Friction/Prevents Mud Loss," *World Oil* (September 1998) **219**, 87.

18. Turki, W. H. and Mackay, A. S.: "Primary Cementing Across Massive Lost Circulation Zones," paper SPE 11490 presented at the 1983 SPE Middle East Oil Technical Conference, Manama, Bahrain, 14-17 March.

19. Sweatman, R., Faul, R., and Ballew, C.: "New Solutions for Subsalt-Well Lost Circulation and Optimized Primary Cementing," paper SPE 56499 presented at the 1999 SPE Annual Technical Conference and Exhibition, Houston, Texas, 3-6 October.

20. Low, N., Daccord, G., and Bedel, J: "Designing Fibered Cement Slurries for Lost Circulation Applications: Case Histories," paper SPE 84617 presented at the 2003 SPE Annual Technical Conference and Exhibition, Denver, Colorado, 5-8 October.

21. Dyke, O. V.: "Cementing in Lost Return Zones," *API Production Practice* (1959) **19**, 201.

22. George, C. R. and Ray, W. D.: "Lost Circulation in Cementing: Causes and Control," *Well Servicing* (May/June 1988) **28**, 20.

23. Brown, A., Davies, M., Nicholson, H., and Gane, B. R.: "The Machar Field, Unlocking the Potential of a North Sea Chalk Field," paper SPE 56974 presented at the 1999 SPE Offshore Europe Conference, Aberdeen, Scotland, 7-9 September.

24. Morita, N., Black, A. D., and Fuh, G.: "Theory of Lost Circulation Pressure," paper SPE 20409 presented at the SPE Annual Technical Conference and Exhibition, New Orleans, Louisiana, 23-26 September.

25. Hamburger, C. L., Tsao, Y., Morrison, B., and Drake, E. N.: "A Shear-Thickening Fluid for Stopping Unwanted Flows While Drilling," *Journal of Petroleum Technology* (March 1985) **37**, 499.

26. Dawson, D. D., Jr. and Goins, W. C., Jr.: "Bentonite-Diesel Oil Squeeze," *World Oil* (October 1953) **137**, 222.

27. Goins, W. G., Jr.: "How To Combat Circulation Loss," *Oil and Gas Journal* (June 1952) **51**, 71.

28. Dawson, D. D., Jr.: "A Study of Lost Circulation in the Gulf Coast," *World Petroleum* (October 1952) **23**, 18.

29. Mata, F. and Veiga, M.: "Crosslinked Cements Solve Lost Circulation Problems," paper SPE 90496 presented at the 2004 SPE Annual Technical Conference and Exhibition, Houston, Texas, 26-29 September.

30. Bruton, J. R., Ivan, C. D., and Heinz, T. J.: "Lost Circulation Control: Evolving Techniques and Strategies to Reduce Downhole Mud Losses," paper SPE 67735 presented at the 2001 SPE/IADC Drilling Conference, Amsterdam, The Netherlands, 27 February – 1 March.

31. Ott, W. K., Miller, W., Sabariman, L., and Mulyadi, S.: "Diversified Uses of A Colloidal Material in Drilling and Completion Operations," *Proceedings* Indonesian Petroleum Association Annual Convention (June 1982), 167.

32. "Rigid Foam Appears to be Good Lost Circulation Material," *Drilling* (September, 1985) **46**, 34.

33. Dupriest, F. E.: Personal Interview. ExxonMobil Development Company, Houston, Texas (January 3, 2005).

34. Meier, J. and Morgan, R.: "Measurement Methods and Models for Characterizing Rheology of HIPRE (High Internal Phase Emulsion) Fracturing Fluids," Halliburton Energy Services, Duncan, Oklahoma (December 17, 2003).

35. Murphy, G.: *Similitude in Engineering*. The Ronald Press Company, New York (1950).

36. Morgan, R. G.: Personal Interview. Halliburton Energy Services, Duncan, Oklahoma (June 8, 2004).

37. Steffe, J. F.: *Rheological Methods in Food Process Engineering*. Second Edition. Freeman Press, East Lansing, Michigan (1996) 109.

38. Morgan, R. G., Steffe, J. F., and Ofoli, R. Y.: "A Generalized Viscosity Model for Extrusion of Protein Doughs," *Journal of Food Process Engineering* (1989) **11**, 55.

39. Walters, H. G., Morgan, R. G., and Harris, P. C.: "Kinetic Rheological Modeling of a Low-Polymer Concentration Fracturing Fluid," paper SPE 71660 presented at the 2001 SPE Annual Technical Conference and Exhibition, New Orleans, Louisiana, 30 September – 3 October.

APPENDIX A

DIMENSIONLESS TERM DERIVATIONS

Table 4 — Dimensionless Term Variable Descriptions

Variable	Description	Dimensions
N	Number of Nozzles	-
D_W	Wellbore Diameter	L
D_N	Nozzle Diameter	L
D_B	Drillbit Diameter	L
ρ_M	Mud Density	ML^{-3}
ρ_{PLIP}	PLIP Density	ML^{-3}
V_M	Mud Velocity	Lt^{-1}
V_{PLIP}	PLIP Velocity	Lt^{-1}
$\mu_{\infty M}$	Mud Plastic Viscosity	$ML^{-1}t^{-1}$
$\mu_{\infty PLIP}$	PLIP Viscosity	$ML^{-1}t^{-1}$
τ_{oM}	Mud Yield Stress	$ML^{-1}t^{-2}$
τ_{oPLIP}	PLIP Yield Stress	$ML^{-1}t^{-2}$

By following the similitude example in Fig. 12, the following dimensionless terms were obtained.

$$k = n - j \| n = 12, j = 3$$
$$k = 12 - 3 = 9$$

Nine dimensionless terms are required to characterize the system although more may exist. Ten dimensionless terms are presented here with the ratio of nozzle diameter to wellbore diameter having little significance and the Pi Mixing Number being most important to the design of the model. **Table 4** shows the variables selected to characterize the dual-flow system.

A.1 Reynolds Number for Mud

$$\Pi_1 = \delta \rho_M^a V_M^b \mu_{\infty M}^c \quad \text{..(A-1)}$$

$$\delta = D_w - D_B \quad \text{..(A-2)}$$

$$M^0 L^0 t^0 = L \left[\frac{M}{L^3} \right]^a \left[\frac{L}{t} \right]^b \left[\frac{M}{Lt} \right]^c \quad \text{..(A-3)}$$

$$M : 0 = a + c \quad \text{..(A-4)}$$

$$L : 0 = 1 - 3a + b - c \quad \text{..(A-5)}$$

$$t : 0 = -b - c \quad \text{..(A-6)}$$

Solving the above equations yields:

$$a = 1 \quad b = 1 \quad c = -1$$

$$\Pi_1 = \frac{\rho_M V_M \delta}{\mu_{\infty M}} = \frac{\rho_M V_M (D_W - D_B)}{\mu_{\infty M}} \quad \text{..(A-7)}$$

A.2 Reynolds Number for PLIP

$$\Pi_2 = D_N \rho_{PLIP}^a V_{PLIP}^b \mu_{\infty PLIP}^c \quad \text{..(A-8)}$$

$$M^0 L^0 t^0 = L \left[\frac{M}{L^3} \right]^a \left[\frac{L}{t} \right]^b \left[\frac{M}{Lt} \right]^c \quad \text{..(A-9)}$$

$$M : 0 = a + c \quad \text{..(A-10)}$$

$$L : 0 = 1 - 3a + b - c \quad \text{..(A-11)}$$

$$t : 0 = -b - c \quad \text{..(A-12)}$$

Solving the above equations yields:

$$a = 1 \quad b = 1 \quad c = -1$$

$$\Pi_2 = \frac{\rho_{PLIP} V_{PLIP} D_N}{\mu_{\infty PLIP}} \quad \dots\dots\dots\dots\dots\dots\dots\dots\dots\dots\dots\dots\dots\dots\dots\dots\text{(A-13)}$$

A.3 Hedstrom Number for Mud

$$\Pi_3 = \tau_{oM} \rho_M^a \mu_{\infty M}^b D_W^c \quad \dots\dots\dots\dots\dots\dots\dots\dots\dots\dots\dots\dots\dots\text{(A-14)}$$

$$M^0 L^0 t^0 = \left[\frac{M}{Lt^2}\right]\left[\frac{M}{L^3}\right]^a\left[\frac{M}{Lt}\right]^b L^c \quad \dots\dots\dots\dots\dots\dots\dots\dots\dots\text{(A-15)}$$

$$M: 0 = 1 + a + b \quad \dots\dots\dots\dots\dots\dots\dots\dots\dots\dots\dots\dots\dots\dots\text{(A-16)}$$

$$L: 0 = -1 - 3a - b + c \quad \dots\dots\dots\dots\dots\dots\dots\dots\dots\dots\dots\text{(A-17)}$$

$$t: 0 = -2 - b \quad \dots\dots\dots\dots\dots\dots\dots\dots\dots\dots\dots\dots\dots\dots\dots\text{(A-18)}$$

Solving the above equations yields:

$$a = 1 \quad b = -2 \quad c = 2$$

$$\Pi_3 = \frac{\rho_M \tau_{oM} D_w^2}{\mu_{\infty M}^2} \quad \dots\dots\dots\dots\dots\dots\dots\dots\dots\dots\dots\dots\dots\dots\text{(A-19)}$$

A.4 Hedstrom Number for PLIP

$$\Pi_4 = \tau_{oPLIP} \rho_{PLIP}^a \mu_{\infty PLIP}^b D_N^c \quad \dots\dots\dots\dots\dots\dots\dots\dots\dots\dots\dots\text{(A-20)}$$

$$M^0 L^0 t^0 = \left[\frac{M}{Lt^2}\right]\left[\frac{M}{L^3}\right]^a\left[\frac{M}{Lt}\right]^b L^c \quad \dots\dots\dots\dots\dots\dots\dots\dots\dots\text{(A-21)}$$

$$M: 0 = 1 + a + b \quad \dots\dots\dots\dots\dots\dots\dots\dots\dots\dots\dots\dots\dots\dots\text{(A-22)}$$

$$L: 0 = -1 - 3a - b + c \quad \dots\dots\dots\dots\dots\dots\dots\dots\dots\dots\dots\text{(A-23)}$$

$$t: 0 = -2 - b \quad \dots\dots\dots\dots\dots\dots\dots\dots\dots\dots\dots\dots\dots\dots\dots\text{(A-24)}$$

Solving the above equations yields:

$$a = 1 \quad b = -2 \quad c = 2$$

$$\Pi_4 = \frac{\rho_{PLIP}\,\tau_{oPLIP}\,D_N^2}{\mu_{\infty PLIP}^2} \quad \dots\dots\dots\dots\dots\dots\dots\dots\dots\dots\dots\dots\dots\dots\dots\dots\dots\dots\dots\dots\dots \text{(A-25)}$$

A.5 Ratio of Nozzle Diameter to Wellbore Diameter

$$\Pi_5 = D_N D_W^a \rho_{PLIP}^b \mu_{\infty PLIP}^c \quad \dots\dots\dots\dots\dots\dots\dots\dots\dots\dots\dots\dots\dots\dots\dots\dots\dots \text{(A-26)}$$

$$M^0 L^0 t^0 = (L)L^a \left[\frac{M}{L^3}\right]^b \left[\frac{M}{Lt}\right]^c \quad \dots\dots\dots\dots\dots\dots\dots\dots\dots\dots\dots\dots\dots\dots\dots \text{(A-27)}$$

$$M : 0 = b + c \quad \dots\dots\dots\dots\dots\dots\dots\dots\dots\dots\dots\dots\dots\dots\dots\dots\dots\dots\dots\dots\dots\dots \text{(A-28)}$$

$$L : 0 = 1 + a - 3b - c \quad \dots\dots\dots\dots\dots\dots\dots\dots\dots\dots\dots\dots\dots\dots\dots\dots\dots\dots \text{(A-29)}$$

$$t : 0 = -c \quad \dots\dots\dots\dots\dots\dots\dots\dots\dots\dots\dots\dots\dots\dots\dots\dots\dots\dots\dots\dots\dots\dots \text{(A-30)}$$

Solving the above equations yields:

$$a = -1 \quad b = 0 \quad c = 0$$

$$\Pi_5 = \frac{D_N}{D_W} \quad \dots\dots\dots\dots\dots\dots\dots\dots\dots\dots\dots\dots\dots\dots\dots\dots\dots\dots\dots\dots\dots\dots\dots \text{(A-31)}$$

A.6 Ratio of Drill Bit Diameter to Wellbore Diameter

$$\Pi_6 = D_B D_W^a \rho_M^b \mu_{\infty M}^c \quad \dots\dots\dots\dots\dots\dots\dots\dots\dots\dots\dots\dots\dots\dots\dots\dots\dots\dots \text{(A-32)}$$

$$M^0 L^0 t^0 = (L)L^a \left[\frac{M}{L^3}\right]^b \left[\frac{M}{Lt}\right]^c \quad \dots\dots\dots\dots\dots\dots\dots\dots\dots\dots\dots\dots\dots\dots\dots \text{(A-33)}$$

$$M : 0 = b + c \quad \dots\dots\dots\dots\dots\dots\dots\dots\dots\dots\dots\dots\dots\dots\dots\dots\dots\dots\dots\dots\dots\dots \text{(A-34)}$$

$$L : 0 = 1 + a - 3b - c \quad \dots\dots\dots\dots\dots\dots\dots\dots\dots\dots\dots\dots\dots\dots\dots\dots\dots\dots \text{(A-35)}$$

$$t : 0 = -c \qquad \text{(A-36)}$$

Solving the above equations yields:

$$a = -1 \quad b = 0 \quad c = 0$$

$$\Pi_6 = \frac{D_B}{D_W} \qquad \text{(A-37)}$$

A.7 Ratio of Mud YP to PLIP YP

$$\Pi_7 = \tau_{oM} \, \tau_{oPLIP}^a \, \rho_M^b \, \mu_{\infty M}^c \qquad \text{(A-38)}$$

$$M^0 L^0 t^0 = \left[\frac{M}{Lt^2} \right] \left[\frac{M}{Lt^2} \right]^a \left[\frac{M}{L^3} \right]^b \left[\frac{M}{Lt} \right]^c \qquad \text{(A-39)}$$

$$M : 0 = 1 + a + b + c \qquad \text{(A-40)}$$

$$L : 0 = -1 - a - 3b - c \qquad \text{(A-41)}$$

$$t : 0 = -2 - 2a - c \qquad \text{(A-42)}$$

Solving the above equations yields:

$$a = -1 \quad b = 0 \quad c = 0$$

$$\Pi_7 = \frac{\tau_{oM}}{\tau_{oPLIP}} \qquad \text{(A-43)}$$

A.8 Ratio of Mud Density to PLIP Density

$$\Pi_8 = \rho_M \, \rho_{PLIP}^a \, \tau_{oPLIP}^b \, \mu_{\infty PLIP}^c \qquad \text{(A-44)}$$

$$M^0 L^0 t^0 = \left[\frac{M}{L^3} \right] \left[\frac{M}{L^3} \right]^a \left[\frac{M}{Lt^2} \right]^b \left[\frac{M}{Lt} \right]^c \qquad \text{(A-45)}$$

$$M : 0 = 1 + a + b + c \qquad \text{(A-46)}$$

$$L : 0 = -3 - 3a - b - c \quad \text{...}(A\text{-}47)$$

$$t : 0 = -2b - c \quad \text{...}(A\text{-}48)$$

Solving the above equations yields:

$$a = -1 \quad b = 0 \quad c = 0$$

$$\Pi_8 = \frac{\rho_M}{\rho_{PLIP}} \quad \text{...}(A\text{-}49)$$

A.9 Number of Nozzles

$$\Pi_9 = N \quad \text{...}(A\text{-}50)$$

A.10 Pi Mixing Number

$$\Pi_{10} = \rho_{PLIP} V_{PLIP}^a \tau_{oPLIP}^b \mu_{\infty M}^c \quad \text{.........................}(A\text{-}51)$$

$$M^0 L^0 t^0 = \left[\frac{M}{L^3}\right]\left[\frac{L}{t}\right]^a\left[\frac{M}{Lt^2}\right]^b\left[\frac{M}{Lt}\right]^c \quad \text{..................}(A\text{-}52)$$

$$M : 0 = 1 + b + c \quad \text{...}(A\text{-}53)$$

$$L : 0 = -3 + a - b - c \quad \text{..}(A\text{-}54)$$

$$t : 0 = -a - 2b - c \quad \text{..}(A\text{-}55)$$

Solving the above equations yields:

$$a = 2 \quad b = -1 \quad c = 0$$

$$\Pi_{10} = \frac{\rho_{PLIP} V_{PLIP}^2}{\tau_{oPLIP}} \quad \text{..}(A\text{-}56)$$

A.11 Product Solution Function

$$\Pi_{10} = function\ of\left[\Pi_1, \Pi_3, \Pi_4, \Pi_6, \Pi_7, \Pi_8, \Pi_9, \Pi_{10}\right] \quad \text{................}(A\text{-}57)$$

$$\frac{\rho_{PLIP}V_{PLIP}D_N}{\mu_{\infty PLIP}} = function\ of \begin{bmatrix} \dfrac{\rho_M V_M \left(D_W - D_B\right)}{\mu_{\infty M}}, \dfrac{\rho_M \tau_{oM} D_W^2}{\mu_{\infty M}^2}, \dfrac{\rho_{PLIP}\tau_{oPLIP}D_N^2}{\mu_{\infty PLIP}^2}, \\[2ex] \dfrac{D_B}{D_W}, \dfrac{\tau_{oM}}{\tau_{oPLIP}}, \dfrac{\rho_M}{\rho_{PLIP}}, N, \dfrac{\rho_{PLIP}V_{PLIP}^2}{\tau_{oPLIP}} \end{bmatrix} \quad (A\text{-}58)$$

A.12 Independency Check

By using elementary similitude rules, matrix dimension values can be eliminated until one value exists for a specific dimension.[35]   If this process of elimination is successful, then a sufficient number of variables to characterize the system have been chosen, and the variables are independent. **Table 5** shows the variable independency check for the wellbore scale model.

Table 5 — Variable Independency Check

According to the same methodology, **table 6** was established showing the independency of the dimensionless terms.

Table 6 — Dimensionless Term Independency Check

Variables	N	R_{eM}	R_{ePLIP}	H_{eM}	H_{ePLIP}	PMN	D_B/D_W	τ_{oM}/τ_{oPLIP}	ρ_M/ρ_{PLIP}
N	1								
D_W				-2			-1		
D_N			1	-2					
D_B									
ρ_M									1
ρ_{PLIP}					1				
V_M		1							
V_{PLIP}						2			
$\mu_{\infty M}$			-2						
$\mu_{\infty PLIP}$				2					
τ_{oM}								1	
τ_{oPLIP}									

APPENDIX B

ADDITIONAL EQUATIONS

B.1 Yield Point Conversion

$$YP_{Pascals} = 101(YP_{Ounces})$$ .... (B-1)

B.2 Reacted Product Density

$$\rho_{RP} = \frac{\rho_{PLIP} + \rho_M}{2}$$ .... (B-2)

B.3 PLIP Velocity

$$V_{PLIP} = \frac{576(\dot{Q}_{PLIP})}{\pi N(D_N^2)}$$ .... (B-3)

B.4 Mud Velocity

$$V_M = \frac{\dot{Q}_M}{\pi(D_W - D_B)^2}$$ .... (B-4)

B.5 Reacted Product Velocity

$$V_{RP} = \frac{\dot{Q}(A_W)}{224.4}$$ .... (B-5)

B.6 Reacted Product Viscosity

$$\mu_{\infty RP} = A\left(YP_{RP}\right)^{B} \quad \text{..} \quad \text{(B-6)}$$

B.7 Hydraulic Radius

$$R_{H} = \frac{A_{CS}}{P_{W}} \quad \text{..} \quad \text{(B-7)}$$

APPENDIX C

FLUID SYSTEM A DATA AND RESULTS

Table 7 — Fluid System A – Scaled Model Test Matrix

Description	Value	Units
A	0.04	-
B	1	-
Wellbore Area	0.0491	[ft^2]
Eff. Mix Length	2	[ft]
P-expontent	1	-
Δt, Bit	0.15	[sec]
Δt, Annulus	0.15	[sec]
Δt, Thief	0.6	[sec]
Δt, Screen	0.6	[sec]
# of Screen Holes	130	-
Radius of Hole	0.0313	[in]

Flow Rate Correlation		
Full Scale	Model	Units
31.5	5	[gal/min]
62.5	10	[gal/min]
94	15	[gal/min]
125	20	[gal/min]

Flow Rate	Velocity	Test	Yield Point at 30 [min]				
[gal/min]	[ft/sec]	-	[Ounces]			Average	[Ratio]
5	17.0	Screen	1.4	1.4	1.4	1.4	0.1
10	34.0	Screen	9.7	11.8	14.0	11.8	1.2
15	51.1	Screen	16.4	15.9	17.1	16.5	1.7
20	68.1	Screen	20.0	19.6	20.3	20.0	2.1
5	17.0	No Screen	0.3	0.6	0.3	0.4	0.0
10	34.0	No Screen	6.8	8.2	5.9	7.0	0.7
15	51.1	No Screen	10.5	9.8	11.1	10.5	1.1
20	68.1	No Screen	13.2	13.2	13.2	13.2	1.4

* Note 20 [gal/min] Yield Point is extrapolated from the other three points

Table 8 — Fluid System A – Scaled Model Data Analysis

Fluid Properties										Pilot Calculations					
Density		Velocity			Yield Point			Plastic Viscosity		Shear Rate				ISH	
[lb/gal]		[m/sec]		[ft/sec]	[Ratio]			[Pascals·sec]		[1/sec]				-	
PLIP	RP	PLIP	Mud	RP	PLIP	RP - Screen	RP- No Screen	PLIP	RP	Bit	Annulus	Thief	Screen	No Screen	Screen
9.3	11.15	5.18	2.50	0.45	0.02	0.15	0.04	0.068	5.66	8159.60	392.19	49.02	1537.22	1312.18	2234.51
9.3	11.15	10.36	4.97	0.91	0.02	1.25	0.73	0.068	47.81	16319.20	784.37	98.05	3074.43	2624.36	4469.02
9.3	11.15	15.57	7.47	1.36	0.02	1.74	1.10	0.068	66.53	24526.80	1176.56	147.07	4611.65	3943.75	6710.73
9.3	11.15	20.76	9.97	1.82	0.02	2.11	1.39	0.068	80.67	32686.40	1568.74	196.09	6148.86	5255.93	8945.24

Table 9 — Fluid System A – ISH* - PMN Correlation Data

ISH*		Yield Point [Ratio]				PMN
Model	B - P	Screen	No Screen	Blender	Predicted	
2.23	1.59	0.15	0.04	0.64	0.60	0.78
4.47	4.29	1.25	0.73	1.16	1.27	3.12
6.71	8.81	1.74	1.10	1.81	2.06	7.02
8.95	13.02	2.11	1.39	2.23	2.52	12.49
1.31	25.91			2.62	3.13	
2.62	1.15			0.47	0.47	
3.94	3.25			0.78	1.04	
5.26	6.59			1.53	1.72	
	9.69			1.59	2.17	
	19.67			2.22	2.93	
	0.84			0.44	0.37	
	2.12			0.77	0.75	
	4.39			1.52	1.30	
	6.47			1.54	1.70	
	12.84			2.47	2.50	
	0.40			0.21	0.23	
	1.05			0.33	0.44	
	2.20			0.70	0.77	
	3.17			1.03	1.02	
	5.97			2.46	1.61	

*Integral Shear History has been divided by 10^3 for convenience

APPENDIX D

FLUID SYSTEM B DATA AND RESULTS

Table 10 — Fluid System B – Blender Test Matrix

Description	Value	Units
Volume	700	[cc]
Mass	1.092	[kg]
P-exponent	1.11	-
K_1	0.11	-
alpha	0.00005	
beta	1.5	-
Ypoo	4.7	[Ratio]

Hand Stir	
Yield Point	**Units**
0.08	[Ratio]
0	[RPM]

Test ID	Mixing Time	RPM	Shear Rate	ISH	Yield Point				
-	[sec]	-	[1/sec]	-	Measurements [Ounces]			*Average*	Predicted
					1	2	3	[Ratio]	[Ratio]
1	2	9640	1060.40	4563.53	5.30	5.50	5.40	0.57	-
2	5	9850	1083.50	11685.04	8.50	8.70	9.20	0.93	-
3	10	9510	1046.10	22476.37	12.90	13.10	12.20	1.34	-
4	15	10120	1113.20	36123.31	17.20	19.00	18.10	1.91	-
5	30	9850	1083.50	70110.22	25.10	24.80	23.20	2.57	-
6	2	7206	792.66	3303.82	7.50	7.90	7.40	0.80	0.36
7	5	7458	820.38	8580.78	12.70	13.30	12.90	1.37	1.04
8	10	7908	869.88	18314.70	15.40	16.30	16.60	1.70	2.23
9	15	7840	862.40	27209.96	25.50	24.00	20.10	2.45	3.04
10	30	7830	861.30	54342.89	40.90	40.60	35.50	4.11	4.25
11	2	5402	594.22	2399.45	4.40	4.10	4.80	0.47	0.26
12	5	5870	645.70	6578.16	8.10	7.40	7.30	0.80	0.77
13	10	5880	646.80	13181.19	12.50	12.70	13.10	1.35	1.63
14	15	5880	646.80	19771.79	21.90	20.60	21.10	2.24	2.38
15	30	5840	642.40	39245.10	31.90	35.20	31.60	3.47	3.76
16	2	3800	418.00	1623.81	2.10	1.80	2.00	0.21	0.18
17	5	3840	422.40	4106.99	3.80	4.10	4.00	0.42	0.45
18	10	3980	437.80	8547.05	7.80	7.50	7.70	0.81	1.03
19	15	3820	420.20	12249.76	14.10	14.00	13.70	1.47	1.52
20	30	3830	421.30	24570.71	23.10	22.80	25.00	2.49	2.83
21	2	1840	202.40	725.98	1.60	1.20	2.40	0.18	0.12
22	5	1910	210.10	1891.75	2.10	3.20	3.20	0.30	0.21
23	10	1980	217.80	3937.71	3.50	4.10	3.60	0.39	0.43
24	15	1920	211.20	5708.23	7.10	6.90	7.70	0.76	0.66
25	30	2090	229.90	12543.81	16.10	15.20	14.70	1.62	1.55

Table 11 — Fluid System B – Scaled Model Test Matrix

Description	Value	Units
A	0.04	-
B	1	-
Wellbore Area	0.0491	[ft^2]
Eff. Mix Length	2	[ft]
P-expontent	1.11	-
Δt, Bit	0.11	[sec]
Δt, Annulus	0.11	[sec]
Δt, Thief	0.7	[sec]
Δt, Screen	0.7	[sec]
# of Screen Holes	130	-
Radius of Hole	0.0313	[in]

Flow Rate Correlation		
Full Scale	Model	Units
31.5	5	[gal/min]
62.5	10	[gal/min]
94	15	[gal/min]
125	20	[gal/min]

Flow Rate	Velocity	Test	Yield Point at 30 [min]				
[gal/min]	[ft/sec]	-	[Ounces]			Average	[Ratio]
5	17.0	Screen	1.4	1.7	1.2	1.4	0.2
10	34.0	Screen	9.7	9.4	9.4	9.5	1.0
15	51.1	Screen	20.8	17.2	19.3	19.1	2.0
20	68.1	Screen	27.5	27.5	27.5	27.5	2.9
5	17.0	No Screen	0.6	0.5	0.5	0.5	0.1
10	34.0	No Screen	2.8	3.2	3.2	3.1	0.3
15	51.1	No Screen	6.8	6.2	6.1	6.4	0.7
20	68.1	No Screen	10.2	10.9	11.5	10.9	1.1

* Note 20 [gal/min] Yield Point is extrapolated from the other three points

Table 12 — Fluid System B – Scaled Model Data Analysis

Fluid Properties								Pilot Calculations							
Density		Velocity			Yield Point			Plastic Viscosity		Shear Rate				ISH	
[lb/gal]		[m/sec]	[m/sec]	[ft/sec]	[Ratio]			[Pascals sec]		[1/sec]				-	
PLIP	RP	PLIP	Mud	RP	PLIP	RP - Screen	RP- No Screen	PLIP	RP	Bit	Annulus	Thief	Screen	No Screen	Screen
9.3	11.15	5.18	2.50	0.45	0.02	0.15	0.06	0.068	0.01	8159.60	392.19	49.02	1537.22	2553.25	4965.22
9.3	11.15	10.36	4.97	0.91	0.02	1.00	0.32	0.068	0.04	16319.20	784.37	98.05	3074.43	5511.07	10717.22
9.3	11.15	15.57	7.47	1.36	0.02	2.01	0.67	0.068	0.08	24526.80	1176.56	147.07	4611.65	8861.46	16826.88
9.3	11.15	20.76	9.97	1.82	0.02	2.90	1.15	0.068	0.12	32686.40	1568.74	196.09	6148.86	11913.79	23151.04

Table 13 — Fluid System B – ISH* - PMN Correlation Data

ISH*		Yield Point [Ratio]				PMN
Model	B - P*	Screen	No Screen	Blender	Predicted	
4.97	3.30	0.15	0.06	0.80	0.36	0.78
10.72	8.58	1.00	0.32	1.37	1.04	3.12
16.83	18.31	2.01	0.67	1.70	2.23	7.02
23.15	27.21	2.90	1.15	2.45	3.04	12.49
2.55	54.34			4.11	4.25	
5.51	2.40			0.47	0.26	
8.66	6.58			0.80	0.77	
11.91	13.18			1.35	1.63	
	19.77			2.24	2.38	
	39.25			3.47	3.76	
	1.62			0.21	0.18	
	4.11			0.42	0.45	
	8.55			0.81	1.03	
	12.25			1.47	1.52	
	24.57			2.49	2.83	
	0.73			0.18	0.12	
	1.89			0.30	0.21	
	3.94			0.39	0.43	
	5.71			0.76	0.66	
	12.54			1.62	1.55	

*Integral Shear History has been divided by 10^3 for convenience
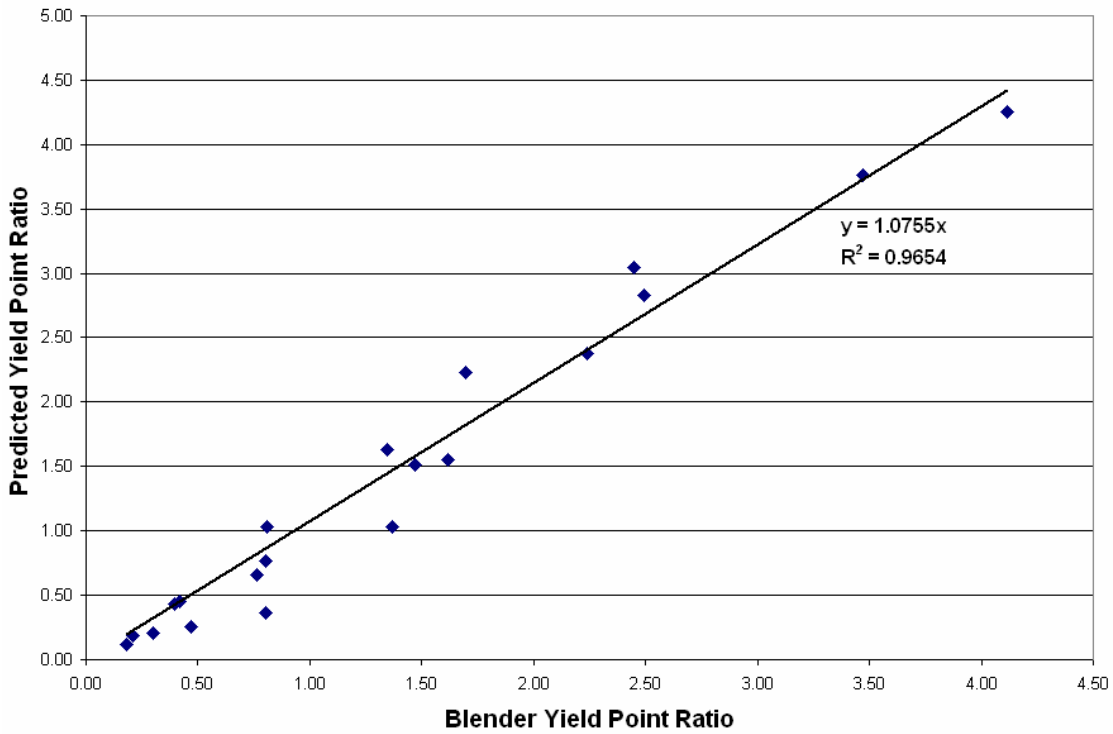
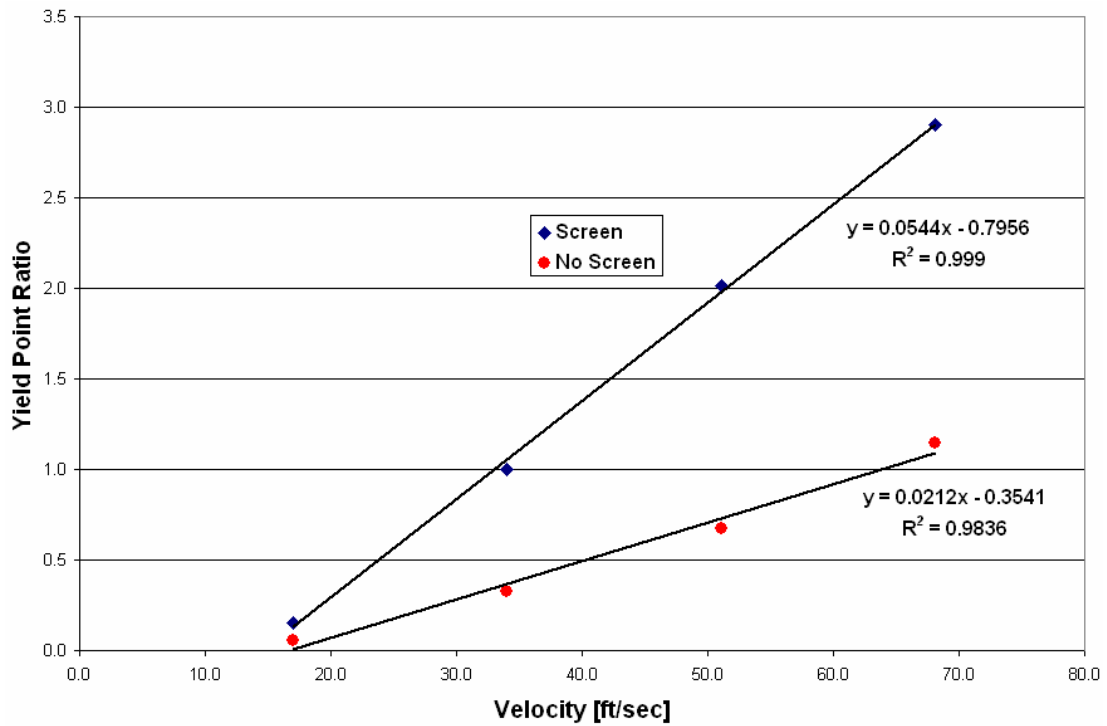**Fig. 24 — Fluid System B – predicted and blender YP comparison.**

Fig. 25 — Fluid System B – pilot scale increase in YP with increasing nozzle velocity.
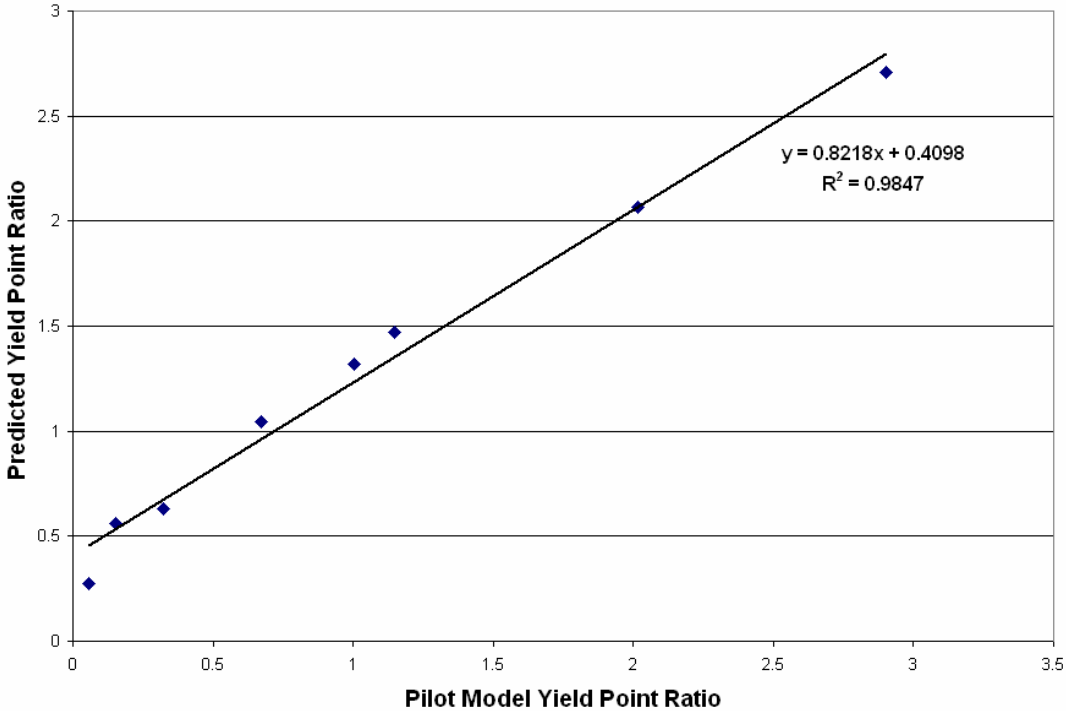
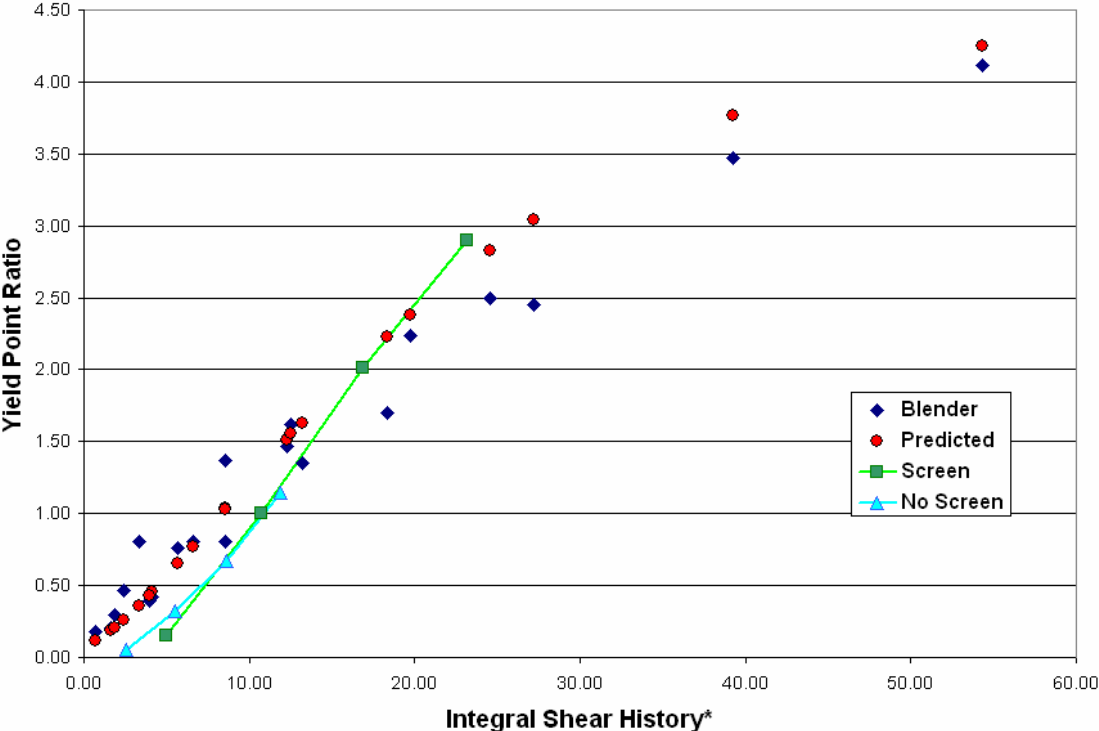Fig. 26 — Fluid System B – predicted and pilot model YP comparison.

$y = 0.8218x + 0.4098$
$R^2 = 0.9847$

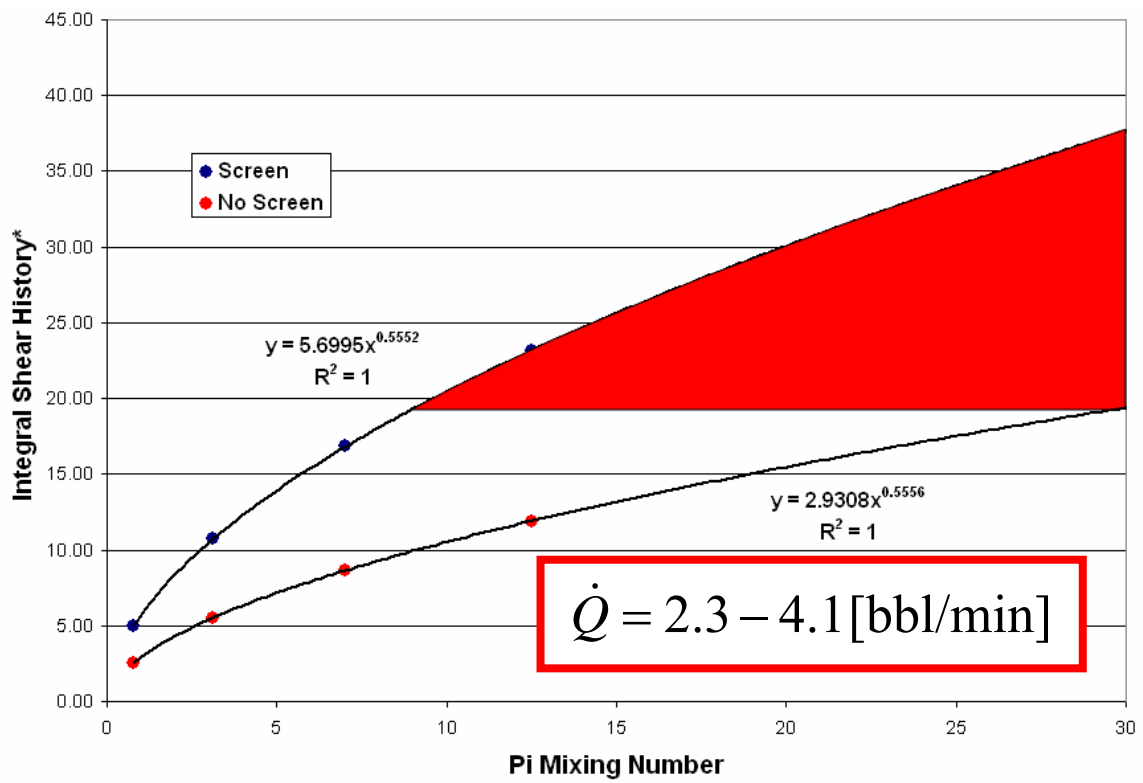Fig. 27 — Fluid System B – effect of ISH on YP during all tests.

Fig. 28 — Fluid System B – ISH - PMN correlation.

APPENDIX E

FLUID SYSTEM C DATA AND RESULTS

Table 14 — Fluid System C – Blender Test Matrix

Description	Value	Units
Volume	700	[cc]
Mass	1.092	[kg]
P-exponent	1.2	-
K₁	0.11	-
alpha	0.000006	
beta	0.2	-
Ypoo	4.70	[Ratio]

Hand Stir	
Yield Point	Units
0.09	[Ratio]
0	[RPM]

Test ID	Mixing Time	RPM	Tip Speed	Shear Rate	ISH	Yield Point				
-	[sec]	-	[ft/sec]	[1/sec]	-	Measurements [Ounces]			Average	Predicted
						1	2	3	[Ratio]	[Ratio]
1	2	7910	69.03	870.10	6737.72	10.70	9.90	11.50	0.54	2.51
2	5	7950	69.38	874.50	16946.57	22.10	23.50	23.20	1.16	2.98
3	10	7882	68.78	867.02	33545.55	30.60	28.40	29.30	1.49	3.37
4	15	7890	68.85	867.90	50379.62	29.60	30.20	29.50	1.50	3.61
5	30	7920	69.12	871.20	101219.15	36.20	37.10	35.50	1.83	4.03
6	2	5730	50.00	630.30	4576.01	8.90	11.10	10.60	0.52	2.33
7	5	5890	51.40	647.90	11824.41	21.20	22.40	22.10	1.11	2.79
8	10	6120	53.41	673.20	24761.27	28.70	25.10	24.10	1.31	3.19
9	15	5820	50.79	640.20	34967.94	28.70	30.90	27.50	1.47	3.40
10	30	5900	51.49	649.00	71091.04	33.70	31.20	33.10	1.65	3.82
11	2	3920	34.21	431.20	2901.65	6.10	6.90	7.50	0.35	2.14
12	5	3940	34.38	433.40	7298.55	20.00	17.60	18.80	0.95	2.55
13	10	3780	32.99	415.80	13888.69	29.40	28.70	31.90	1.52	2.87
14	15	3900	34.03	429.00	21629.18	32.30	29.20	31.90	1.57	3.12
15	30	3920	34.21	431.20	43524.70	32.60	31.90	30.50	1.60	3.53
16	2	1790	15.62	196.90	1132.73	5.00	5.00	5.10	0.25	1.79
17	5	1990	17.37	218.90	3215.62	6.00	6.50	7.40	0.33	2.18
18	10	1960	17.10	215.60	6315.07	26.10	27.60	27.00	1.36	2.48
19	15	1900	16.58	209.00	9125.71	30.50	27.60	28.10	1.45	2.66
20	30	1930	16.84	212.30	18597.79	30.90	30.90	30.90	1.56	3.03

Table 15 — Fluid System C – Scaled Model Test Matrix

Description	Value	Units
A	0.04	-
B	1	-
Wellbore Area	0.0491	[ft^2]
Eff. Mix Length	2	[ft]
P-expontent	1.2	-
Δt, Bit	0.25	[sec]
Δt, Annulus	0.25	[sec]
Δt, Thief	0.7	[sec]
Δt, Screen	0.7	[sec]
# of Screen Holes	130	-
Radius of Hole	0.0313	[in]

Flow Rate Correlation		
Full Scale	Model	Units
31.5	5	[gal/min]
62.5	10	[gal/min]
94	15	[gal/min]
125	20	[gal/min]

Flow Rate	Velocity	Test	Yield Point at 30 [min]				
[gal/min]	[ft/sec]	-	[Ounces]			Average	[Ratio]
5	17.0	Screen	28.6	30.9	29.1	29.5	3.1
10	34.0	Screen	30.6	34.1	33.7	32.8	3.5
15	51.1	Screen	37.0	34.5	33.9	35.1	3.7
20	68.1	Screen	37.8	37.8	37.8	37.8	4.0
5	17.0	No Screen	29.1	28.7	28.4	28.7	3.0
10	34.0	No Screen	28.7	32.3	29.6	30.2	3.2
15	51.1	No Screen	32.3	32.1	34.5	33.0	3.5
20	68.1	No Screen	34.1	35.8	36.3	35.4	3.7

* Note 20 [gal/min] Yield Point is extrapolated from the other three points

Table 16 — Fluid System C – Scaled Model Data

Fluid Properties											
Density		Velocity			Yield Point			Plastic Viscosity	
[lb/gal]		[m/sec]		[ft/sec]	[Pascals]			[Pascals sec]	
PLIP	RP	PLIP	Mud	RP	PLIP	RP - Screen	RP- No Screen	PLIP	RP
9.3	11.15	5.18	2.50	0.45	19.15	3.12	3.03	0.068	0.12
9.3	11.15	10.36	4.97	0.91	19.15	3.46	3.19	0.068	0.14
9.3	11.15	15.57	7.47	1.36	19.15	3.71	3.48	0.068	0.15
9.3	11.15	20.76	9.97	1.82	19.15	3.99	3.73	0.068	0.16

Pilot Calculations						
Shear Rate				ISH	
[1/sec]				-	
Bit	Annulus	Thief	Screen	No Screen	Screen
8159.60	392.19	49.02	1537.22	12756.28	17424.80
16319.20	784.37	98.05	3074.43	29306.24	40031.69
24526.80	1176.56	147.07	4611.65	47781.37	65228.54
32686.40	1568.74	196.09	6148.86	67443.17	92083.79

Table 17 — Fluid System C – ISH* - PMN Correlation Data

ISH*		Yield Point [Ratio]				PMN
Model	B - P	Screen	No Screen	Blender	Predicted	
17.42	6.74	3.12	3.03	1.13	2.51	0.78
40.03	16.95	3.46	3.19	2.42	2.98	3.12
65.23	33.55	3.71	3.48	3.11	3.37	7.02
92.08	50.38	3.99	3.73	3.14	3.61	12.49
12.76	101.22			3.83	4.03	
29.31	4.58			1.08	2.33	
47.78	11.82			2.31	2.79	
67.44	24.76			2.74	3.19	
	34.97			3.06	3.40	
	71.09			3.45	3.82	
	2.90			0.72	2.14	
	7.30			1.98	2.55	
	13.89			3.16	2.87	
	21.63			3.28	3.12	
	43.52			3.34	3.53	
	1.13			0.53	1.79	
	3.22			0.70	2.18	
	6.32			2.84	2.48	
	9.13			3.03	2.66	
	18.60			3.26	3.03	

*Integral Shear History has been divided by 10^3 for convenience
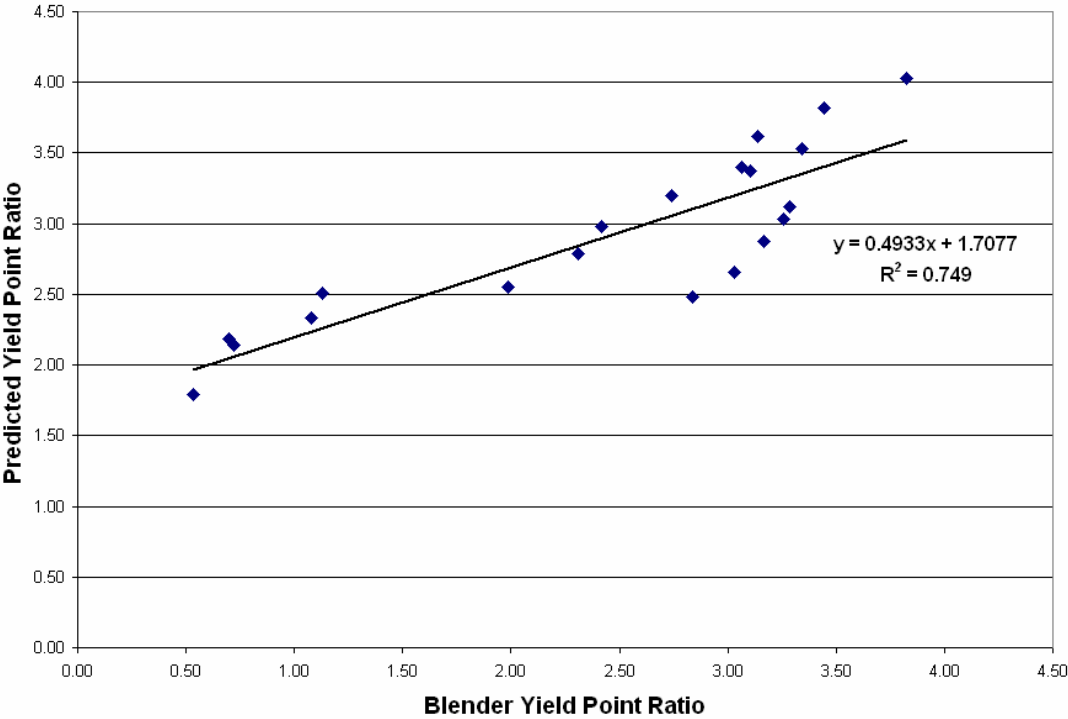
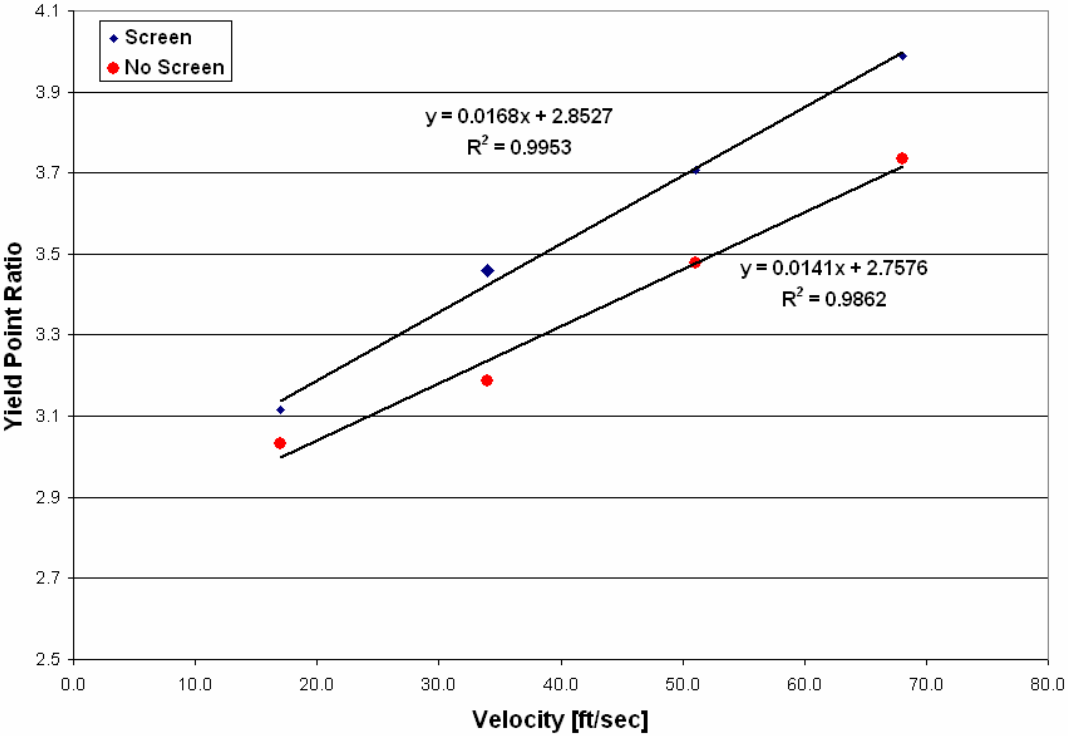**Fig. 29 — Fluid System C – predicted and blender YP comparison.**

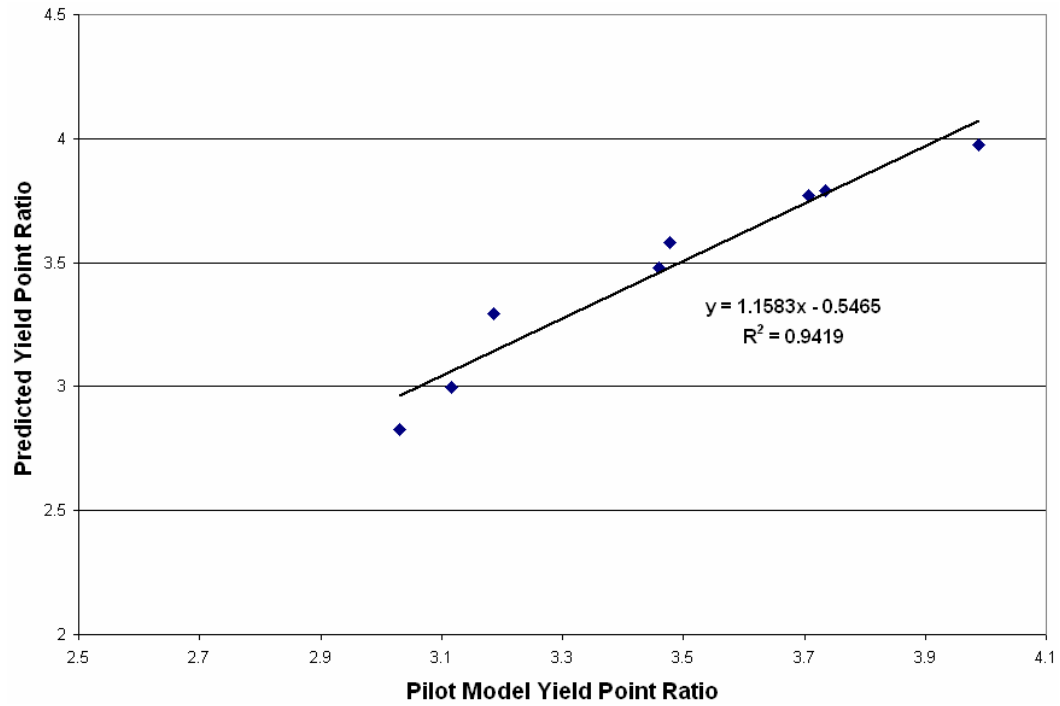**Fig. 30 — Fluid System C – pilot scale increase in YP with increasing nozzle velocity.**

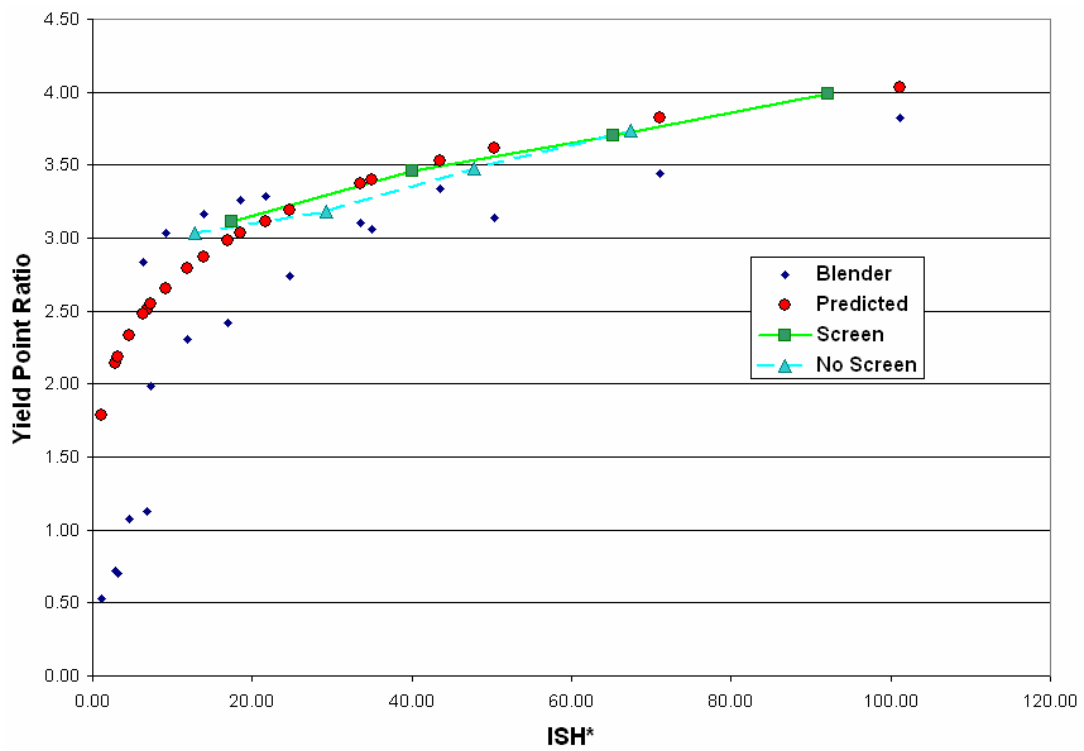**Fig. 31 — Fluid System C – predicted and pilot model YP comparison.**

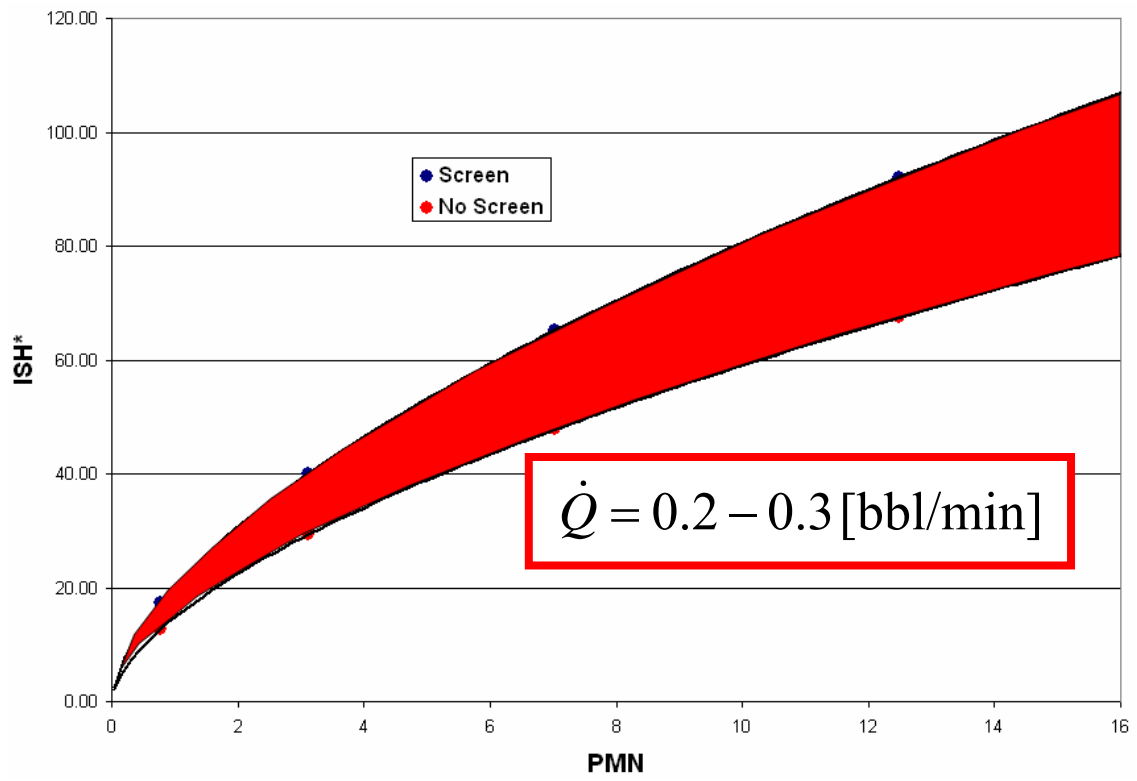**Fig. 32 — Fluid System C – effect of ISH on YP during all tests.**

Fig. 33 — Fluid System C – ISH- PMN correlation.

APPENDIX F

SHEAR RATE DATA

Table 18 — Shear Rate Data Analysis

Known Data		
Description	Value	Units
Sample Size	700	[cc]
Ta	75	[degF]
Viscosity	0.757	[Pascal sec]
Specific Heat	0.5	[Cal/(g degC)]
Density	0.89	[g/cc]
n'	1	-

Shear Rate Data				Calculations							
Mixing Time		Temperature	RPM	$\Delta T,i$	$\Delta t,i$	$(\Delta T,i)/(\Delta t,i)$	T,i,ave	$(T,i,ave-T,a)$	RPM	$(\Delta T/\Delta t),0$	VASR
[min]	[sec]	degF	-	[degF]	[sec]	[degF/sec]	[degF]	[degF]	-	[deg F/sec]	[1/sec]
0	0	78	0	2	60	0.033	79	4	2000	0.035	218.510
1	60	80	2000	7	240	0.029	83.5	8.5	4000	0.086	343.807
5	300	87	2000	7	300	0.023	90.5	15.5	6000	0.189	509.036
10	600	94	2000	7	300	0.023	97.5	22.5	0	0	0
15	900	101	2000	5	300	0.017	103.5	28.5			
20	1200	106	2000								
0	0	75	0	5	60	0.083	77.5	2.5			
1	60	80	4000	18	240	0.075	89	14			
5	300	98	4000	12	300	0.040	104	29			
10	600	110	4000	10	300	0.033	115	40			
15	900	120	4000	9	300	0.030	124.5	49.5			
20	1200	129	4000								
0	0	76	0	11	60	0.183	81.5	6.5			
1	60	87	6000	34	240	0.142	104	29			
5	300	121	6000	23	300	0.077	132.5	57.5			
10	600	144	6000	15	300	0.050	151.5	76.5			
15	900	159	6000	14	300	0.047	166	91			
20	1200	173	6000								

Table 19 — Fan Viscometer Calculations

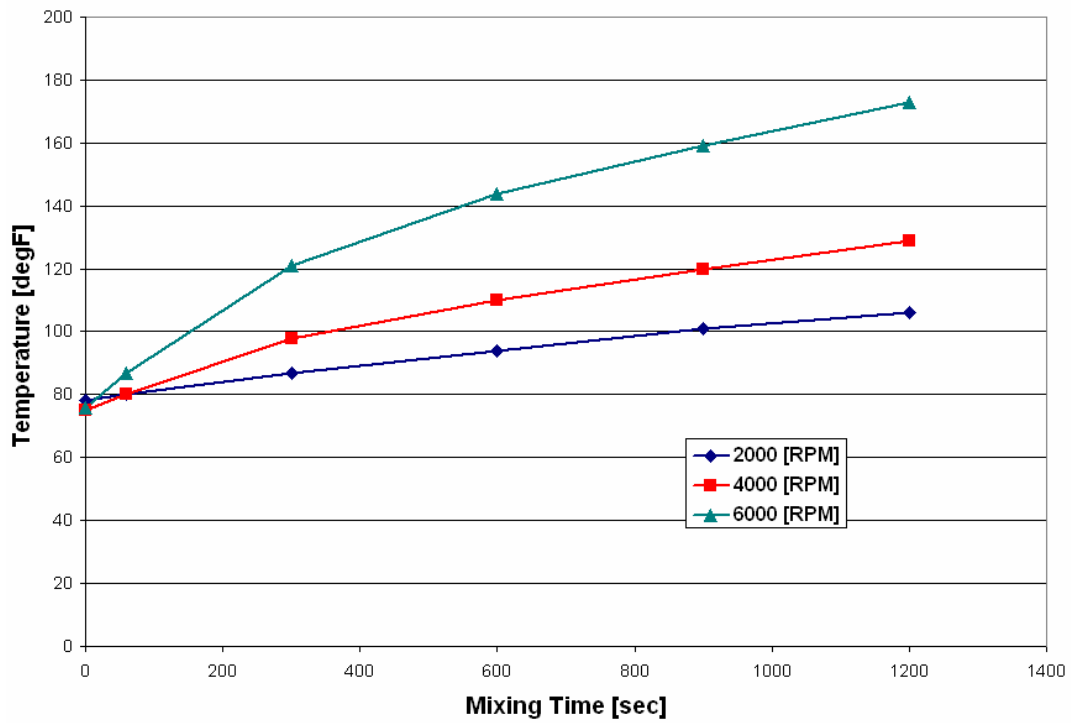| Fann Viscometer Calculations				
[RPM]	Dial Reading	Viscosity		
-	-	[cp]	[Pascal sec]	Average
R_{100}	244	732	0.732	0.757
R_{60}	146	730	0.730	
R_{30}	74	740	0.740	
R_{10}	25	738	0.738	
R_{6}	16	800	0.800	
R_{3}	8	800	0.800	

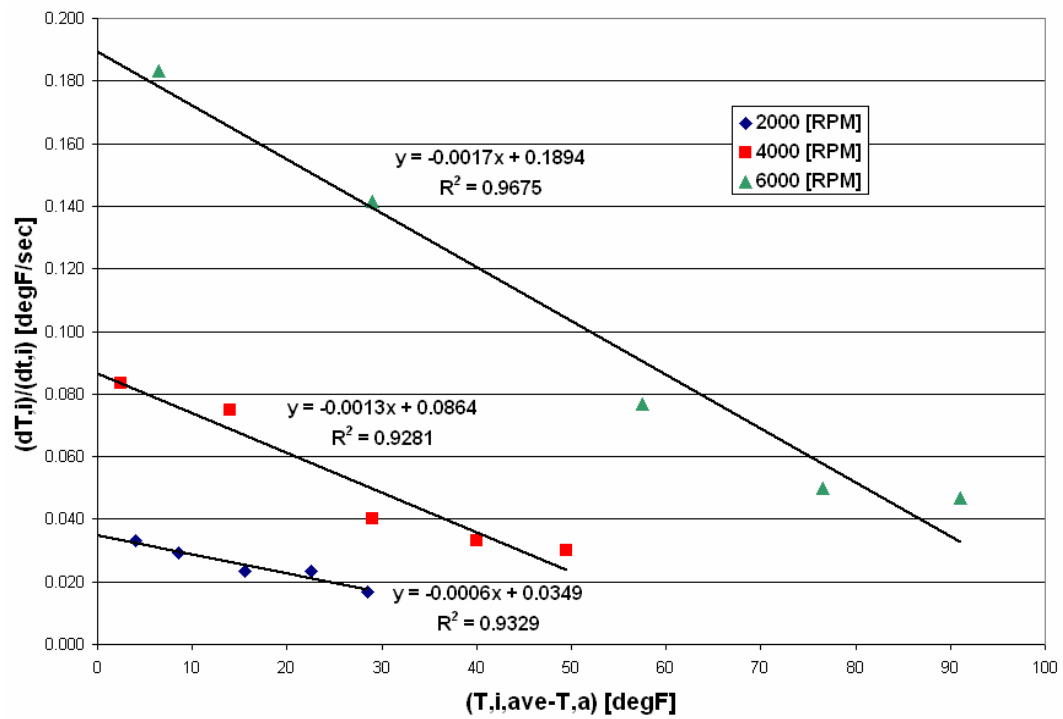**Fig. 34 — Temperature variation at specific RPMs.**

Fig. 35 — Y-intercept analysis.

VITA

I was born in Humble, Texas on December 9, 1980. I was raised in a small town just north of my birthplace and moved to College Station, Texas, in 1999 to attend college. I received my Bachelor of Science degree in mechanical engineering at Texas A&M University, College Station, Texas in 2003 and immediately enrolled in graduate school where in May 2005 I received my Master of Science degree in petroleum engineering. I am currently employed at ExxonMobil Development Company as a drilling engineer in Houston, Texas. I plan to pursue a doctoral degree in petroleum engineering beginning summer 2005.

My permanent address is:

Robert Derryl Massingill, Jr.

21163 Velma Lane

Porter, Texas 77365